Phenomenological $pp \rightarrow d\pi^+$ model of $A(\vec{p},\pi^+)B$ reactions

W. R. Falk
Department of Physics, University of Manitoba, Winnipeg, Manitoba, Canada R3T 2N2
(Received 6 January 1994)

A phenomenological $pp \rightarrow d\pi^+$ model of $A(\vec{p},\pi^+)B$ reactions is developed that incorporates the full spin dependence of the former reaction. The model makes predictions of analyzing powers and differential cross sections and is applied to an investigation of the $(\vec{p},\pi^+)$ reaction on ^{2}H, ^{3}He, ^{4}He, and ^{12}C. The general trends of the predicted observables agree reasonably well with experiment for the helium isotopes. Much greater sensitivity due to effects of absorption and interference between different amplitudes is observed for carbon. Nevertheless, characteristic features of the analyzing powers and differential cross sections for single-particle and two-particle–one-hole states are clearly discerned. Consistent cross section normalization factors between the model and experiment, of the order of unity, are found in nearly all cases over the whole range of nuclei and energies investigated.

PACS number(s): 25.40.Qa, 24.10.−i, 21.45.+v, 24.70.+s

I. INTRODUCTION

Since the pioneering investigations of exclusive nuclear pion production at CERN [1,2] and Uppsala [3] over 20 years ago, much effort has been devoted to characterizing these reactions experimentally and in elucidating the basic processes and mechanisms involved. These investigations, comprising measurements of the angular distributions of the differential cross sections and analyzing powers over a wide range of bombarding energies, have covered many nuclei and involved many different final states. While a wealth of data has been accumulated, the shear richness and variety of the results have defied an overall understanding and systematic interpretation. Several comprehensive overviews giving the status of this field as of more than a decade ago have appeared in review articles [4–6] and in the proceedings of a conference [7]. Many of the questions and issues raised in these articles have not been resolved to date. To cite one simple example, a general feature that is presently not understood is the dependence of the cross section on target mass number at fixed bombarding energy. More specific characteristics pertaining to individual angular distributions of the differential cross sections and analyzing powers are also not understood at all in terms of an overall theoretical framework.

Modern microscopic models of the $A(\vec{p},\pi^+)B$ reaction have been developed in recent years by a number of different groups [8–11]. These models are also among the first to include analyzing power as a calculated observable, although some earlier models have done so as well [12]. Each of these models tends to introduce the basic physics in somewhat different ways and, depending on the assumptions and emphases, has been applied to different studies. Thus the model of Alons *et al.* [8] has been applied to a study on ^{3}He [13,14], that of Iqbal and Walker to ^{12}C [9,15], and that of Cooper and Matsuyama [10] to ^{16}O [16]. Intercomparisons of the different treatments and assumptions made in these models have thus been difficult to make. Within their respective areas of applications, these models have had a certain measure of success. However, some unifying overview of the many features displayed by the $A(\vec{p},\pi^+)B$ reaction has not emerged from these models.

In the experimental realm, progress in our understanding of nuclear pion production has come from facilities that provided high-quality polarized proton beams coupled with high-resolution spectrometer systems. Representative of such recent results are those from IUCF [17], TRIUMF [15,16,18], and LAMPF [19,20]. These measurements have added a wealth of detail, not only because of the numerous final states amenable to study in high-resolution experiments, but also because of extensive analyzing power data that have been accumulated. A rather consistent pattern that has emerged is that in the $(\vec{p},\pi^+)$ reaction, especially near threshold ($\approx$ 200 MeV), the analyzing powers have a character that is very much like that of the $pp \rightarrow d\pi^+$ reaction. Indeed, this feature was noted in the earliest analyzing power data recorded for this reaction [21]. Such a two-nucleon $pp \rightarrow d\pi^+$ mechanism has become a cornerstone for the qualitative interpretation [17] of extensive data on pion production on ^{12,13}C. The selectivity and strength of the $(\vec{p},\pi^-)$ reaction, which has been documented for many different cases as well [22,17], is also understood qualitatively in terms of a two-nucleon mechanism, where the allowed $NN \rightarrow NN\pi$ channels are much more restricted than for $(\vec{p},\pi^+)$.

Support for a $pp \rightarrow d\pi^+$ two-nucleon mechanism in $(\vec{p},\pi^+)$ reactions is found in other measurements as well. The energy dependence of the $(\vec{p},\pi^+)$ differential cross section at fixed momentum transfer has been investigated on a number of nuclei [15,23] from 200 to 500 MeV and has been shown to follow closely the energy dependence of the free $pp \rightarrow d\pi^+$ reaction. Inclusive measurements in the ^{12}C$(p,\pi^+)X$ reaction [24] of both cross sections and analyzing powers at 400 and 450 MeV are consistent with a simple quasifree model that assumes an underlying $NN \rightarrow NN\pi^+$ production mechanism. Indeed, a recent coincidence study [25] of the reaction ^{12}C$(p,d\pi^+)^{11}$B at

223 MeV has shown that the results are in remarkable agreement with distorted wave impulse approximation (DWIA) calculations. This provides very strong support to the picture of quasifree pion production, mediated by the elementary $pp \rightarrow d\pi^+$ process. Furthermore, new pion absorption measurements [26] at 115 MeV in the reaction $^{16}O(\pi^+,pp)$, over an extended region of phase space, demonstrate that two-nucleon absorption is dominant. The $\pi^+ + np \rightarrow pp$ process accounts for 76% of the total absorption cross section, comprising absorption not only on p-shell nucleon pairs, but also s-p nucleon pairs.

Dominance of the $pp \rightarrow d\pi^+$ elementary process over other $NN \rightarrow NN\pi^+$ processes follows from the much greater cross section of the former reaction near threshold. The $NN \rightarrow NN\pi$ reaction cross sections are usually expressed in terms of the isospin of the NN pair in the initial and final channels as follows [27]:

$$pp \rightarrow d\pi^+, \quad \sigma_{10}^d ,$$

$$pp \rightarrow pn\pi^+, \quad \sigma_{10} + \sigma_{11} ,$$

$$pn \rightarrow nn\pi^+, \quad \tfrac{1}{2}(\sigma_{11} + \sigma_{01}) ,$$

$$pn \rightarrow pp\pi^-, \quad \tfrac{1}{2}(\sigma_{11} + \sigma_{01}) .$$

In this terminology, σ_{10}^d dominates for bombarding energies up to 525 MeV, beyond which energy σ_{10} continues to increase rapidly, while σ_{10}^d reaches a peak at 585 MeV and then begins to drop with increasing energy [27]. On the other hand, σ_{11} is much smaller for energies less than 550 MeV, and σ_{01} remains poorly defined, but is smaller yet than σ_{11}.

Formulating expressions for the $A(\vec{p},\pi^+)B$ reaction observables in terms of the $pp \rightarrow d\pi^+$ reaction is not a new idea. Ruderman [28] formulated expressions for the differential cross sections for the reactions $p + d \rightarrow \pi^+ + {}^3H$ and $p + d \rightarrow \pi^0 + {}^3He$ in terms of the $pp \rightarrow d\pi^+$ reaction cross section. A generalization of this approach was subsequently used by Ingram *et al.* [29] in deriving expressions for the $A(p,\pi^+)B$ reaction. Further developments of this approach were made by Fearing [30] who added distortions in the incident and outgoing channels. Most recently, Kurath [31] has applied a closely related approach with special emphasis on the nuclear structure aspects as it pertains to the target nuclei $^{12,13}C$. Common to all these approaches is that only the cross section observable is calculated in the models.

Given the very important information carried by the analyzing power and the extensive data presently available regarding this observable, a new formulation of a $pp \rightarrow d\pi^+$ model was undertaken that incorporates detailed experimental information on this reaction. The development follows that of Ingram *et al.* [29] except for the inclusion of spin and the considerable attendant complications that this entails. The goal of this endeavor is an attempt to correlate as extensive a body of data as possible under the umbrella of a simple model. In Sec. II the details of this formulation are given. Section III discusses the implementation and general features of the model, and in Sec. IV the predictions of this model for the target nuclei ^2H, ^3He, ^4He, and ^{12}C are presented and discussed.

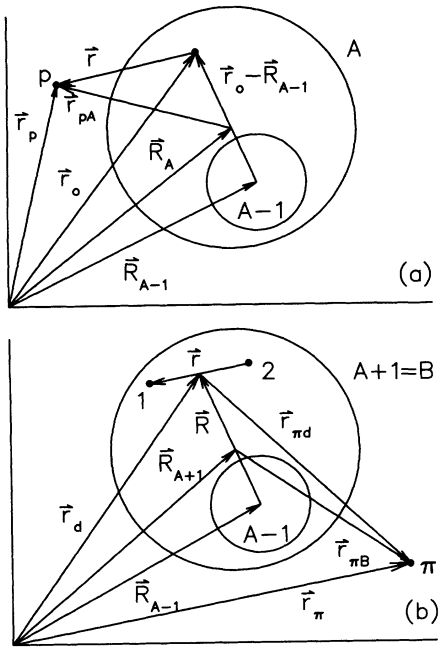

FIG. 1. Schematic representation of coordinates for the $A(\vec{p},\pi^+)B$ reaction in the (a) incident and (b) outgoing channels.

II. $pp \rightarrow d\pi^+$ MODEL

A. Formulation

In this section an expression is derived for the matrix element for the $A(\vec{p},\pi^+)B$ reaction in terms of the matrix element for the $pp \rightarrow d\pi^+$ reaction. For clarity, all the spin information will be suppressed for the time being; these details will be discussed in full in Sec. II B. Unless specified otherwise, all quantities refer to the $(p + A)$ center-of-mass (c.m.) system.

Since the pp interaction depends on the momenta of the two protons, the momentum of the struck target proton will be indicated explicitly. The target nucleus wave function is thus expressed as a product wave function of a proton and $A - 1$ nucleons as follows:

$$\begin{aligned}\psi_A &= \psi_{A-1}(\vec{\xi}_{A-1}) \otimes \psi_0(\vec{r}_0 - \vec{R}_{A-1}) \\ &= \psi_{A-1}(\vec{\xi}_{A-1}) \otimes (1/2\pi)^{3/2} \int \phi(\vec{k}_0) e^{i\vec{k}_0 \cdot (\vec{r}_0 - \vec{R}_{A-1})} d^3\vec{k}_0 \, . \end{aligned} \tag{1}$$

In the last line above, the proton wave function has been represented by its Fourier transform and the meaning of the various spatial coordinates is illustrated in Fig. 1(a). Vector coupling of the core to the single proton is indicated by

the symbol $\otimes$. Introducing plane waves for the motion of p and A,

$$e^{i\vec{k}_p\cdot\vec{r}_p}e^{-i\vec{k}_p\cdot\vec{R}_A}\ , \tag{2}$$

with

$$\vec{R}_A=\left(\frac{A-1}{A}\right)\vec{R}_{A-1}+\vec{r}_0/A\ , \tag{3}$$

the incident channel wave function becomes

$$\Psi_{pA}=(1/2\pi)^{3/2}\psi_{A-1}(\vec{\xi}_{A-1})\otimes\int\phi(\vec{k}_0)\exp\left(-i\left[\frac{A-1}{A}\vec{k}_p+\vec{k}_0\right]\cdot\vec{R}_{A-1}\right)e^{i\vec{k}_p\cdot\vec{r}_p}e^{i[\vec{k}_0-\vec{k}_p/A]\cdot\vec{r}_0}d^3\vec{k}_0\ . \tag{4}$$

Here $\vec{k}_p$ and $\vec{k}_0-\vec{k}_p/A$ are the momenta of the incident and struck proton in the $(p+A)$ c.m. frame, respectively. It is assumed that momentum is conserved in the $pp\rightarrow d\pi^+$ reaction. Hence

$$\vec{K}=\left(\frac{A-1}{A}\right)\vec{k}_p+\vec{k}_0=\vec{k}_\pi+\vec{k}_d\ , \tag{5}$$

where $\vec{K}$ is the total momentum of the two interacting protons and $\vec{k}_\pi$ and $\vec{k}_d$ the momenta of the resulting pion and deuteron, respectively. The plane waves for the two protons are next expressed in terms of their total momentum $\vec{K}$ and their relative momentum $\vec{k}_{pp}$. Thus with $\vec{r}=\vec{r}_p-\vec{r}_0$, $\vec{r}_d=(\vec{r}_p+\vec{r}_0)/2$, and the result (3), one obtains

$$\begin{aligned}e^{i\vec{k}_p\cdot\vec{r}_p}e^{i[\vec{k}_0-\vec{k}_p/A]\cdot\vec{r}_0}&=e^{i\vec{K}\cdot\vec{r}_d}e^{i\vec{k}_{pp}\cdot\vec{r}}\\&=e^{i(\vec{k}_d+\vec{k}_\pi)\cdot\vec{r}_d}e^{i\vec{k}_{pp}\cdot\vec{r}}\ .\end{aligned} \tag{6}$$

For the outgoing channel comprising a pion and nucleus B (with $B\equiv A+1$), one has, referring to Fig. 1(b),

$$\begin{aligned}\vec{r}_d&=\vec{R}_{A-1}+\vec{R},\\ \vec{R}_{A+1}&=\vec{R}_{A-1}+\left(\frac{2}{A+1}\right)\vec{R}=\vec{r}_d-\left(\frac{A-1}{A+1}\right)\vec{R}\ .\end{aligned} \tag{7}$$

In a similar manner as before, plane waves are introduced for the motion of π^+ and B, which, after some rearranging, can be expressed as

$$\begin{aligned}&e^{i\vec{k}_\pi\cdot\vec{r}_\pi}e^{-i\vec{k}_\pi\cdot\vec{R}_{A+1}}\\&\quad=e^{i\vec{k}_\pi\cdot\vec{r}_\pi}e^{i\vec{k}_d\cdot\vec{r}_d}e^{-i\vec{q}\cdot\vec{R}}\\&\qquad\times\exp\left(-i\left[\frac{A-1}{A}\vec{k}_p+\vec{k}_0\right]\cdot\vec{R}_{A-1}\right)\ .\end{aligned} \tag{8}$$

In this expression the quantity $\vec{q}$ has been introduced; it represents the momentum of the two-nucleon pn system (i.e., the recaptured deuteron) in the final nucleus B and is given by

$$\vec{q}=\left(\frac{A-1}{A}\right)\vec{k}_p+\vec{k}_0-\left(\frac{A-1}{A+1}\right)\vec{k}_\pi\ . \tag{9}$$

It will prove convenient to express the internal wave function of nucleus B as a product wave function of the nucleus $(A-1)$ and two nucleons. Furthermore, the two-nucleon wave function is expressed in terms of the internal coordinate $\vec{r}$ and the relative coordinate $\vec{R}$ of the two-nucleon cluster with respect to nucleus $(A-1)$. Thus

$$\psi_{A+1}=\psi_{A-1}(\vec{\xi}_{A-1})\otimes\psi(\vec{R})\otimes\psi(\vec{r})\approx\psi_{A-1}(\vec{\xi}_{A-1})\otimes\psi(\vec{R})\otimes\left\{\left[\frac{\psi(r)}{\psi_d(r)}\right]_{r=a}\psi_d(\vec{r})\right\}\ . \tag{10}$$

In the last step above, the pn relative emotion wave function $\psi(\vec{r})$ has effectively been replaced by the deuteron internal wave function $\psi_d(\vec{r})$. This has been done in order that the latter wave function can be introduced into the $pp\rightarrow d\pi^+$ matrix element. Since the pp interaction is assumed to be of short range, the ratio of these two wave functions may be evaluated at some small value of a (or, alternatively, normalized in the interval $0\leq r\leq a$). This ratio is defined as γ. The foregoing assumptions and the form of the expression also imply that the angular part has been restricted to angular momentum zero.

Combining these results, the outgoing channel wave function becomes

$$\Psi_{\pi B}=\psi_{A-1}(\vec{\xi}_{A-1})\otimes\psi(\vec{R})\gamma e^{-i\vec{q}\cdot\vec{R}}\exp\left(-i\left[\frac{A-1}{A}\vec{k}_0+\vec{k}_1\right]\cdot\vec{R}_{A-1}\right)\otimes\psi_d(\vec{r})e^{i\vec{k}_\pi\cdot\vec{r}_\pi}e^{i\vec{k}_d\cdot\vec{r}_d}\ . \tag{11}$$

Introducing the results from the previous expressions, the matrix element for the $A(\vec{p},\pi^+)B$ reaction is obtained. Integrations must be carried out over the $3A$ internal coordinates [32] of nucleus B and the coordinates of the pion. The integrations over the $3(A-2)$ core coordinates are immediate, yielding the result

$$\langle \pi^+ B|T_{pp\to d\pi^+}|pA\rangle = \gamma(1/2\pi)^{3/2}\int d^3\vec{k}_0\phi(\vec{k}_0)\int d^3\vec{R}\,\psi^*(\vec{R})e^{i\vec{q}\cdot\vec{R}}\langle d\pi^+|T_{01}|pp\rangle\ , \tag{12}$$

where

$$\langle d\pi^+|T_{01}|pp\rangle = \int d^3\vec{r}_{\pi d}d^3\vec{r}\,e^{-i\vec{k}_\pi\cdot\vec{r}_{\pi d}}\psi_d^*(\vec{r})[T_{01}]e^{i\vec{k}_{pp}\cdot\vec{r}} \tag{13}$$

is the matrix element for the $pp \to d\pi^+$ reaction, representing the NN isospin transition $1 \to 0$. The main features linking the matrix elements for the $pp \to d\pi^+$ and $A(\vec{p},\pi^+)B$ reactions are the integration over the momentum distribution of the struck target proton and the Fourier transform of the recaptured pn pair in the final nucleus.

B. Angular momentum and isospin couplings

In the following development, the system C (with $C \equiv A-1$) will be referred to as the core. The coordinates of the two nucleons with respect to C are $\vec{\rho}_p = \vec{r}_p - \vec{R}_{A-1}$ and $\vec{\rho} = \vec{r}_0 - \vec{R}_{A-1}$. The angular momentum and spin coupling details follow. Single-particle states are specified by their values of n, l, and j. The total isospin and its projection quantum number will be indicated by T (or t, where $t = \frac{1}{2}$) and N (or t_3, where $t_3 = \frac{1}{2}$), respectively. The target nucleus wave function in the form of Eq. (1) is then

$$\begin{aligned}\psi_A \to \psi^{J_AT_A}_{M_AN_A}(\vec{\xi}_C,\vec{\rho}) &= \Sigma^{nlj\ J_C\ T_C}_{\lambda m M_C N_C \mu_0}\zeta_{AC}(nljt)(T_CN_Ctt_3|T_AN_A)\\ &\times(J_CM_Cjm|J_AM_A)(l\lambda\tfrac{1}{2}\mu_0|jm)\\ &\times\psi^{J_CT_Cnlj}_{M_CN_C}(\vec{\xi}_C)\psi^{nlj}_m(\rho)Y^\lambda_l(\hat{\rho})\chi^{1/2}_{\mu_0}\ .\end{aligned} \tag{14}$$

The expansion coefficients ζ_{AC} are closely related to single-particle coefficients of fractional parentage [32], which yield this expansion in terms of separately antisymmetrized product wave functions. Furthermore, they are related to the single-particle spectroscopic amplitudes $S^{1/2}_{AC}(1)$ by the expression $\zeta_{AC} = S^{1/2}_{AC}(1)\binom{A}{1}^{-1/2}$, where $\binom{A}{1}$ is the combinatorial factor. $S_{AC}(1)$ is the usual single-particle spectroscopic factor. If different configurations are present in the nuclear wave function, the coefficients ζ_{AC} must be further multiplied by the respective amplitudes of these components. The spin function of the target proton is given by $\chi^{1/2}_{\mu_0}$.

The wave function of the final nucleus B is most conveniently expressed in cluster form comprising a deuteron (d) and core (C) as follows:

$$\begin{aligned}\psi_B \to \psi^{J_BT_B}_{M_BN_B}(\vec{\xi}_C,\vec{R},\vec{r}) &= \Sigma^{J\ T\ J_C\ T_C\ S}_{M\ N\ M_C\ N_C\ \Lambda\Sigma}\zeta_{BC}(LSJT)(T_CN_CTN|T_BN_B)\\ &\times(J_CM_CJM|J_BM_B)(L\Lambda S\Sigma|JM)\\ &\times\psi^L_\Lambda(\vec{R})\psi_{d\,\Sigma N}^{ST}(\vec{r})\ .\end{aligned} \tag{15}$$

This form is most suitable for very light nuclei.

Alternatively, if shell model wave functions of harmonic oscillator form are used, the formalism developed for two-nucleon transfer reactions by Towner and Hardy [33] is more appropriate. In this case one writes

$$\begin{aligned}\psi_B \to \psi^{J_BT_B}_{M_BN_B}(\vec{\xi}_C,\vec{\rho}_1,\vec{\rho}_2) &= \Sigma^{[n_1l_1j_1][n_2l_2j_2]\ J\ T\ J_C\ T_C}_{M\ N\ M_C\ N_C}\zeta_{BC}\{[n_1l_1j_1][n_2l_2j_2];JT\}\\ &\times(T_CN_CTN|T_BN_B)(J_CM_CJM|J_BM_B)\\ &\times\psi^{J_CT_C}_{M_CN_C}(\vec{\xi}_C)\psi^{j_1j_2\ J\ T}_{M\ N}(\vec{\rho}_1,\vec{\rho}_2)\ ,\end{aligned} \tag{16}$$

where $\vec{\rho}_1$ and $\vec{\rho}_2$ are the coordinates of the two nucleons with respect to the core C. Here two-nucleon expansion coefficients ζ_{BC} have been introduced, which, in this latter case, are closely related to two-particle coefficients of fractional parentage [33]. In analogy with the single-particle case, these coefficients are related to the two-particle spectroscopic amplitudes $S^{1/2}_{BC}(2)$ by the expression $\zeta_{BC} = S^{1/2}_{BC}(2)\binom{A+1}{2}^{-1/2}$. The two-nucleon, or pair wave function, and the core wave function are separately antisymmetrized. The pair wave function, expressed in jj coupling above, is next recoupled into LS form:

$$\psi^{j_1j_2\ J\ T}_{M\ N}(\vec{\rho}_1,\vec{\rho}_2) = \sum_{L,S}\begin{bmatrix} l_1 & l_2 & L\\ \frac{1}{2} & \frac{1}{2} & L\\ j_1 & j_2 & J\end{bmatrix}\psi^{l_1l_2LS\ J\ T}_{M\ N}(\vec{\rho}_1,\vec{\rho}_2)\ . \tag{17}$$

The square brackets [ ] denote a normalized 9-J coefficient [33]. The LS coupled pair wave function in terms of its spin and spatial parts is

$$\psi^{l_1l_2LSJT}_{M\ N}(\vec{\rho}_2,\vec{\rho}_2) = \Sigma_{\Lambda\Sigma}(L\Lambda S\Sigma|JM)\psi^{l_1l_2\ L}_\Lambda(\vec{\rho}_1,\vec{\rho}_2)\chi^{ST}_{\Sigma N}\ . \tag{18}$$

A Moshinsky transformation [33] is now applied to the spatial part of the pair wave function to yield an expression in terms of the internucleon coordinate $\vec{r}$ and the coordinate of the c.m. of the pair with respect to the c.m. of the core, $\vec{R}$. The result is

$$\begin{aligned}\psi^{l_1l_2\ L}_\Lambda(\vec{\rho}_1,\vec{\rho}_2) &= g\Sigma_{\lambda_1\lambda_2}(l_1\lambda_1l_2\lambda_2|L\Lambda)\psi^{[n_1l_1j_1]}_{\lambda_1}(\vec{\rho}_1)\psi^{[n_2l_2j_2]}_{\lambda_2}(\vec{\rho}_2)\\ &= g\Sigma^{n'\ l'\ N'\ L'}_{\lambda'\ \Lambda'}\langle n_1l_1n_2l_2,L\|N'L'n'l',L\rangle\\ &\times(L'\Lambda'l'\lambda'|L\Lambda)\psi^{n'\ l'}_{\lambda'}(\vec{r})\psi^{N'\ L'}_{\Lambda'}(\vec{R})\ .\end{aligned} \tag{19}$$

The Moshinsky bracket is indicated by the symbol $\langle\|\rangle$. Antisymmetrization between the two nucleons results in the factor g, which has a value of 1 if $[n_1l_1j_1] \equiv [n_2l_2j_2]$ and a value $\sqrt{2}$ otherwise. Orbital angular momentum coupling satisfies the relationship $\vec{L}' + \vec{l}' = \vec{l}_1 + \vec{l}_2$, where $\vec{L}'$ is the orbital angular momentum of the pair with respect to C and $\vec{l}'$ the internal orbital angular momentum of the pair. Conservation of harmonic oscillator quanta restricts the sum above to

$$2n_1 + l_1 + 2n_2 + l_2 = 2n' + l' + 2N' + L' \,. \tag{20}$$

It is helpful at this stage to assume that the two-nucleon cluster will be restricted to carry the quantum numbers of the deuteron and, furthermore, that the deuteron D state can be ignored. Thus $S = 1$, $T = 0$, and $l' = 0$. As a consequence, $L' = L$ and $\Lambda' = \Lambda$ and the sums simplify considerably, to yield

$$\begin{aligned}\psi^{l_1 l_2 L}_{\Lambda}(\vec{\rho}_1, \vec{\rho}_2) &= g\Sigma^{n'N'}\langle n_1 l_1 n_2 l_2, L\|N' L n' 0, L\rangle \\ &\quad\times[H_{n'0}(\nu_B r^2/2)Y_0^0(\hat{r})][H_{N'L}(2\nu_B R^2)Y_L^{\Lambda}(\hat{R})] \,.\end{aligned} \tag{21}$$

The radial oscillator functions, designated by H, are characterized by the parameters $\nu_B/2$ and $2\nu_B$, respectively, for the internal and relative motion of the pn pair, where ν_B is the oscillator parameter for the nucleus B. The term in the last square brackets is to be identified with the function $\psi(\vec{R})$ defined in the previous section, whereas the other term in the square brackets relates to $\psi(\vec{r})$ as follows:

$$\begin{aligned}\psi(\vec{r}) &\to \left\{\left[\frac{\psi(r)}{\psi_d(r)}\right]_{r=a}\psi_d(\vec{r})\right\} \\ &= \left\{\left[\frac{H_{n'0}(\nu_B r^2/2)}{\psi_d(r)}\right]_{r=a}[\psi_d(r)Y_0^0(\hat{r})\chi^{10}_{\Sigma 0}]\right\} \,.\end{aligned} \tag{22}$$

A Hulthen form for the radial part of the deuteron wave function $\psi_d(r)$ was used with parameters $\alpha = 0.2316$ fm^{-1} and $\beta = 1.232$ fm^{-1}. Normalization of the harmonic oscillator and deuteron wave functions was effected by integrating over the interval $0 \le r \le a$, with $a \approx 1.5$ fm. This normalization depends on ν_B and n' and is designated $\gamma_{n'}$. For n' equal to 0 and 1, $\gamma_{n'}$ has values of 0.79 and 0.84, respectively, for $\nu_B = 0.311$ fm^{-2} (appropriate for ^{12}C, say).

C. Matrix element

Using standard techniques for evaluating the Fourier transforms, the momentum wave function in (1) is written as

$$\begin{aligned}\phi(\vec{k}_0) &= (1/2\pi)^{3/2}\int \psi^{nlj}_m(\rho)Y_l^{\lambda}(\hat{\rho})e^{-i\vec{k}_0\cdot\vec{\rho}}d^3\vec{\rho} \\ &= (-i)^l\sqrt{2/\pi}Y_l^{\lambda}(\hat{k}_0)\int \psi^{nlj}_m(\rho)j_l(k_0\rho)\rho^2 d\rho \\ &= (-i)^l\sqrt{2/\pi}Y_l^{\lambda}(\hat{k}_0)I_{nl}(k_0) \,,\end{aligned} \tag{23}$$

where $j_l(k_0\rho)$ is a spherical Bessel function and $I_{nl}(k_0)$ represents the associated radial integral.

The matrix element appearing in Eq. (12) can now be expressed in detail in terms of all the angular momentum and isospin couplings. Since $T = 0$ for the transferred pair, $T_C = T_B$. A factor A results from the number of terms in the nuclear overlap integral and a statistical weighting factor of $\sqrt{A+1}$ from the number of direct terms [32] in the matrix element. This latter factor arises from antisymmetrization between the incident proton and the target nucleons. Assembling the appropriate equations,

$$\begin{aligned}\langle\vec{k}_\pi M_B|T_{pp\to d\pi^+}|\vec{k}_p\mu_p M_A\rangle &= A\sqrt{A+1}\sum_{\mu_0\Sigma}\Bigg\langle \Sigma^{nlj\,J_C\;J\;Ln'N'[n_1l_1j_1][n_2l_2j_2]}_{\lambda m M_C M\Lambda}\gamma_{n'}\zeta_{AC}(nljt) \\ &\quad\times(T_B N_B t t_3|T_A N_A)(J_C M_C jm|J_A M_A)(l\lambda\tfrac{1}{2}\mu_0|jm) \\ &\quad\times\{(-i)^l/(2\pi^2)\}\int d^3\vec{k}_0 Y_l^{\lambda}(\hat{k}_0)I_{nl}(k_0) \\ &\quad\times\zeta_{BC}\{[n_1l_1j_1][n_2l_2j_2]; JT=0\}(J_C M_C JM|J_B M_B) \\ &\quad\times\begin{bmatrix} l_1 & l_2 & L \\ \frac{1}{2} & \frac{1}{2} & 1 \\ j_1 & j_2 & J\end{bmatrix}(L\Lambda 1\Sigma|JM)g\langle n_1l_1n_2l_2, L\|N'Ln'0, L\rangle \\ &\quad\times\int d^3\vec{R}\,e^{i\vec{q}\cdot\vec{R}}[H_{N'L}(2\nu_B R^2)Y_L^{\Lambda^*}(\hat{R})]\langle\vec{k}_\pi\Sigma|T_{01}|\vec{k}_{pp}\mu_p\mu_0\rangle\Bigg\rangle \\ &\equiv \sum_{\mu_0\Sigma}\int d^3\vec{k}_0\{F(\vec{k}_p\vec{k}_\pi\vec{k}_0\mu_p\mu_0\Sigma M_A M_B)\langle\vec{k}_\pi\Sigma|T_{01}|\vec{k}_{pp}\mu_p\mu_0\rangle\} \,.\end{aligned} \tag{24}$$

Here

$$\langle \vec{k}_\pi \Sigma | T_{01} | \vec{k}_{pp} \mu_p \mu_0 \rangle = \int d^3\vec{r}_{\pi d} d^3\vec{r}\, e^{-i\vec{k}_\pi \cdot \vec{r}_{\pi d}} \psi_d(r) Y_0^0(\hat{r}) [T_{01}(\mu_p \mu_0 \Sigma)] e^{i\vec{k}_{pp}\cdot\vec{r}}\,. \tag{25}$$

Since $\vec{k}_{pp}$ and $\vec{q}$ depend on $\vec{k}_0$, the matrix element for the $A(\vec{p},\pi^+)B$ reaction depends on numerous lengthy sums and an integral over the matrix element for the $pp \to d\pi^+$ reaction. This latter integral was carried out numerically.

D. Eikonal approximation for distortions

In order to be able to investigate the effects of distortions, an eikonal approximation [34] was introduced to describe the scattering states. This has the effect of modifying the plane waves and appears as a modification to the integral over $d^3\vec{R}$. The plane waves are multiplied by the factors

$$D_p(\vec{R}) = \exp\left[\frac{-i}{\hbar v_p}\int_{-\infty}^{\vec{S}} V_p dz'\right], \quad D_\pi(\vec{R}) = \exp\left[\frac{-i}{\hbar v_\pi}\int_{\vec{S}}^{\infty} V_\pi dz'\right], \tag{26}$$

where $\vec{S} = \{(A-1)/(A+1)\}\vec{R}$ and the integrations are carried out along the undeflected trajectories of the particles. Optical potentials for the particles are designated by V and their velocities in the c.m. by v. The functions D were further approximated by making a multipole expansion in the form

$$D_p(\vec{R}) \approx 4\pi \sum_{k_\mu} U_{pk}(R) Y_k^\mu(\hat{R}) Y_k^{\mu^*}(\hat{k}_p), \tag{27}$$

$$D_\pi(\vec{R}) \approx 4\pi \sum_{j\nu} U_{\pi j}(R) Y_j^\nu(\hat{R}) Y_j^{\nu^*}(\hat{k}_\pi). \tag{28}$$

A good representation for the functions D was obtained for $j,k \le 2$, and polynomials of degree 2 in R, for the functions U. In this form the integral over $d^3\vec{R}$ can be performed using standard techniques alluded to earlier. Taking the incident beam direction as the z axis, the result is

$$\begin{aligned} I^R_{N'L\Lambda}(q) = (4\pi)^{3/2} \sum_{\kappa j k \nu I} & i^\kappa (2k+1)\left[\frac{(2j+1)(2\kappa+1)}{2L+1}\right]^{1/2} (k0j\nu|I\nu) \\ & \times (k0j0|I0)(\kappa\Lambda - \nu I\nu|L\Lambda)(\kappa 0I0|L0) Y_\kappa^{\Lambda-\nu^*}(\hat{q}) Y_j^{\nu^*}(\hat{k}_\pi) \\ & \times \int_0^\infty H_{N'L}(2\nu_B R^2) j_\kappa(qR) U_{pk}(R) U_{\pi j}(R) R^2 dR, \end{aligned} \tag{29}$$

where $j_\kappa(qR)$ is a spherical Bessel function. The radial integral appearing above is analytic in form, comprising a small number of terms. This is also the case for the integral $I_{nl}(k_0)$ defined previously, whether the single-particle wave function is of harmonic oscillator or Hulthen form.

E. Cross sections and analyzing powers

The expression for the partial cross section in the $A(\vec{p},\pi^+)B$ reaction is

$$\left(\frac{d\sigma}{d\Omega}\right)_{pA}^{\mu_p M_A M_B} = \frac{(2\pi)^4}{\beta_{pA}} \rho_{pA} |\langle \vec{k}_\pi M_B | T_{pp\to d\pi^+} | \vec{k}_p \mu_p M_A \rangle|^2, \tag{30}$$

where $\beta_{pA}c$ is the relative velocity of the particles in the incident channel and ρ_{pA} is the final density of states factor given by $p_\pi E_\pi E_B/(E_\pi + E_B)$. A similar expression applies to the $pp \to d\pi^+$ reaction. As a matter of convenience, amplitudes W for the $pp \to d\pi^+$ reaction were defined such that

$$\left(\frac{d\sigma}{d\Omega}\right)_{pp}^{\mu_p \mu_0 \Sigma} = |W(\vec{k}_{pp}\vec{k}_\pi \mu_p \mu_0 \Sigma)|^2. \tag{31}$$

Then

$$\left(\frac{d\sigma}{d\Omega}\right)_{pA}^{\mu_p M_A M_B} = \left|\Sigma_{\mu_0 \Sigma} \int d^3\vec{k}_0 \left[F(\vec{k}_p \vec{k}_\pi \vec{k}_0 \mu_p \mu_0 \Sigma M_A M_B) \left(\frac{\rho_{pA}}{\rho_{pp}^\dagger}\right)^{1/2} \left(\frac{\beta_{pp}^\dagger}{\beta_{pA}}\right)^{1/2} W^\dagger(\vec{k}_{pp}\vec{k}_\pi \mu_p \mu_0 \Sigma)\right]\right|^2 \tag{32}$$

$$\equiv |W_{pA}(\vec{k}_p \vec{k}_\pi \mu_p M_A M_B)|^2. \tag{33}$$

Quantities that are to be evaluated in the pp c.m. frame are indicated by a dagger. In terms of the amplitudes W_{pA} defined by the last equation, the spin averaged cross section is

$$\left(\frac{d\sigma}{d\Omega}\right)_{pA} = \frac{1}{2(2J_A+1)} \sum_{\mu_p M_A M_B} |W_{pA}(\vec{k}_p \vec{k}_\pi \mu_p M_A M_B)|^2, \tag{34}$$

and the analyzing power is

$$(A_{N0})_{pA} = 2\,\mathrm{Im} \frac{\left[\sum_{M_A M_B} W_{pA}(\vec{k}_p \vec{k}_\pi \mu_p^+ M_A M_B) \sum_{M_{A'} M_{B'}} W^*_{pA}(\vec{k}_p \vec{k}_\pi \mu_p^- M_{A'} M_{B'})\right]}{\left[\left|\sum_{M_A M_B} W_{pA}(\vec{k}_p \vec{k}_\pi \mu_p^+ M_A M_B)\right|^2 + \left|\sum_{M_A M_B} W_{pA}(\vec{k}_p \vec{k}_\pi \mu_p^- M_A M_B)\right|^2\right]}. \tag{35}$$

Here μ_p^+ and μ_p^- represent the incident proton spin projections parallel and antiparallel to the z axis.

F. Amplitudes for the $pp \to d\pi^+$ reaction

Amplitudes for the $pp \to d\pi^+$ reaction were obtained from the extensive analyses of Bugg, Hasan, and Shypit [35] covering proton bombarding energies from 305 to 800 MeV. A spline fit as a function of the bombarding energy was made over the entire energy range for the amplitudes a_0 to a_{12} and a_{14}. In addition, a smooth extrapolation of the partial wave amplitudes from 800 to about 900 MeV was made. These amplitudes a are defined in numerous articles (see Refs. [35,36], for example). The quantities W, defined in Eq. (31), were expressed in terms of the above amplitudes. As a confirmation, the $pp \to d\pi^+$ reaction observables were recalculated using these quantities W.

It is well known that the total cross section σ_{10} for the final state where the pn system is unbound exceeds the total cross section σ_{10}^d for the bound pn system for energies above 525 MeV [27]. (The labels 1 and 0 refer to the isospin of the NN pair in the initial and final states, respectively.) As well, it has been demonstrated that the analyzing powers for the $pp \to pn\pi^+$ reaction can be very well accounted for [37] in terms of the analyzing powers for the $pp \to d\pi^+$ reaction for modest internal pn excitation energies. Thus the $pp \to pn\pi^+$ reaction can be expected to make a significant contribution to the $A(\vec{p},\pi^+)B$ reaction. Inclusion of this contribution was introduced with the modification

$$W(\vec{k}_{pp} \vec{k}_\pi \mu_p \mu_0 \Sigma) \to W(\vec{k}_{pp} \vec{k}_\pi \mu_p \mu_0 \Sigma) \left\{1 + \frac{\sigma_{10}^\star}{\sigma_{10}^d}\right\}^{1/2}. \tag{36}$$

The quantity $\sigma_{10}^\star$ represents not the total, but that fraction of the σ_{10} cross section that can be characterized by internal orbital angular momentum $l = 0$ for the pn system. This was estimated from three-body phase space and an S-wave final state interaction enhancement factor [38]. This estimated fraction is shown in Fig. 2. The discussion in Sec. IV will compare calculations with and without this contribution included.

G. Momentum distributions

The momentum sharing which is built into this model mitigates to a considerable degree the demand for detailed knowledge of the high momentum components of the nuclear wave functions. Nevertheless, an adequate representation to values of about 2 fm^{-2} for the single-particle momenta must be used. For the target nucleus ^{2}H, the wave functions of Machleidt, Holinde, and Elster [39] were used. Inclusion of the D state was found to be very important, without which the magnitudes of the analyzing powers were severely underestimated. An alternative Hulthen parametrization for both the S and D states was also used, which yielded very similar results. For ^{3}He a Hulthen-like wave function with parameters adjusted empirically could be obtained which provided a good representation of the proton momentum distribution in ^{3}He, calculated by Schiavilla, Pandharipande, and Wiringa [40], for both the S and D states. The S-state momentum distribution has the form

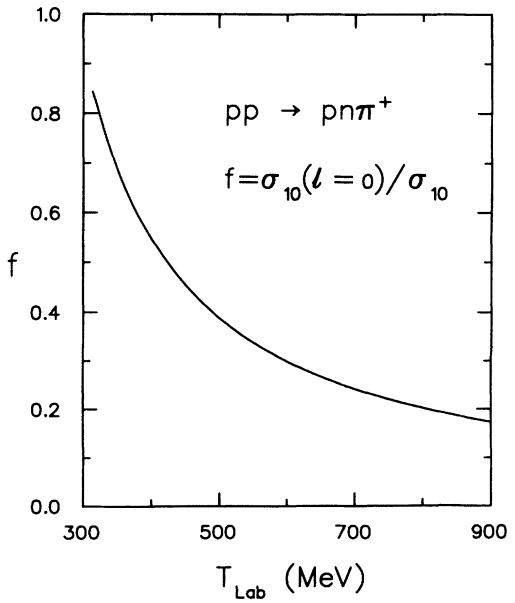

FIG. 2. Estimated fraction of the $pp \to pn\pi^+$ reaction cross section (σ_{10}) that contributes in the $pp \to d\pi^+$ model.

$\phi(k) \propto [1/(k^2+\alpha^2) - 1/(k^2+\beta^2)]$ and is also a good representation of the electron scattering results of Marchand *et al.* [41]. Likewise, for ^{4}He a Hulthen-like parametrization was obtained which provided a good representation of the Schiavilla-Pandharipande-Wiringa [40] S-state momentum distribution. These momentum distributions for ^{3}He and ^{4}He are also in reasonable agreement with experimental distributions obtained from analyses of $(p,2p)$ reactions on these nuclei by Epstein *et al.* [42] and van Oers *et al.* [43], respectively, up to $k = 1.5$ fm^{-1}. Details of the above parameters are given in Table I.

For the target nucleus ^{12}C, harmonic oscillator single-particle states calculated with an oscillator parameter $\nu = \nu_A = \nu_B = 0.311$ fm^{-2} were used. The resulting p-shell momentum distribution is of the form $|\phi(k)|^2 \propto k^2 e^{-k^2/\nu}$, which is, in general, in good agreement with that predicted for the $1p_{3/2}$ shell [44].

Final state $d + C$ relative motion wave functions for the light nuclei were calculated in an harmonic oscillator basis. Since the asymptotic region of these functions drops off too rapidly, they were modified by matching an asymptotic wave function characteristic of the appropriate deuteron separation energy (from the final nucleus) and the angular momentum L. These composite wave functions were then expanded in an harmonic oscillator series.

H. Nuclear structure expansion coefficients

The nuclear structure expansion coefficients used in the calculations, ζ_{AC} and ζ_{BC}, are shown in Table II. These coefficients were calculated from the nuclear overlaps as defined in Refs. [32,33] for pure configurations. Tabulated values include multiplicative factors that account for configuration mixing, if present. The target nuclei ^{2}H and ^{3}He were assumed to have D-state components of 6% and 7%, respectively. For ^{12}C and ^{13}C only the simplest configurations were assumed; nevertheless, it is observed that many different combinations of the struck target nucleon state and the J and L values of the recaptured pn pair enter the calculation.

III. IMPLEMENTATION AND TESTING

The various sums appearing in Eqs. (24) and (29) were most conveniently handled by initially calculating and storing in several large arrays the results of all the possible angular momentum couplings. Nuclear structure information was included in these arrays with a summation over the nuclear structure expansion coefficients that describe the struck target proton and the recaptured pn pair. Numerical integration over the struck proton momentum could then be performed efficiently. Testing of the computer program for carrying out these calculations, in addition to the tests of individual subprograms, involved a simulated $pp \rightarrow d\pi^+$-like calculation where the angular momentum couplings were tested. Faithful reproduction of the $pp \rightarrow d\pi^+$ analyzing powers was obtained.

A. Off-shell effects

Since the $pp \rightarrow d\pi^+$ reaction takes place in a nuclear environment, the process is off shell. Indeed, the momenta $\vec{k}_\pi$ and $\vec{k}_{pp}$ appearing in Eq. (25) are not compatible with the free $pp \rightarrow d\pi^+$ reaction. Within this formulation no unambiguous approach exists by which the on-shell amplitudes for this reaction can be applied to the nuclear environment. Furthermore, in a reaction like (p,π) where threshold effects are very pronounced [45], kinematical considerations play an important role. In the context of this model, a procedure must be devised for mapping the on-shell amplitudes onto the nuclear problem. Several different approaches were incorporated in the program, from which the following were found empirically to be generally most appropriate.

(1) The intermediate recoil nucleus $C = A - 1$ in the initial stage of the reaction was assumed to be on shell; the struck proton, with a momentum p_0, in the rest frame of the target nucleus, was assigned the energy $E_0 = m_A c^2 - (m_C c^2 + p_0^2/2m_C)$.

(2) From the energies and momenta of the two protons, all the requisite kinematical quantities in the pp

TABLE I. Harmonic oscillator (ν) and Hulthen (α,β) parameters characterizing the momentum distributions.

Reaction		Target nucleus $\alpha^2+\beta^2$ (fm^{-2})	Target nucleus $\alpha^2\beta^2$ (fm^{-4})	ν_A (fm^{-2})	Residual nucleus $2\nu_B$ (fm^{-2})
^{2}H$(p,\pi^+)^3$H	S	1.553	0.081		0.234
	D	2.237	0.450		
	S,D[a]				
^{3}He$(p,\pi^+)^4$He	S	0.992	0.142		0.434
	D	0.850	0.176		
^{4}He$(p,\pi^+)^5$He	S	1.027	0.659		0.434
^{12}C$(p,\pi^+)^{13}$C				0.311	0.622

[a]Parameters as given by Machleidt, Holinde, and Elster [39].

c.m. frame [i.e., $\vec{k}_{pp}$ and the quantities appearing in Eq. (32)] were calculated.

(3) The angle between the vectors $\vec{k}_\pi$ and $\vec{k}_{pp}$ was used as the pion scattering angle for evaluation of the $pp \to d\pi^+$ reaction amplitudes.

(4) Finally, and most significantly, the dynamical parameter that defined the energy at which the $pp \to d\pi^+$ reaction amplitudes were evaluated was defined by $\vec{k}_\pi$. Specifically, $\vec{k}_\pi$, the pion momentum in the $(p+A)$ c.m. frame, was also taken as the pion momentum in the free $pp \to d\pi^+$ reaction. This has the effect of shifting upwards the energy scale at which the $pp \to d\pi^+$ amplitudes are calculated. By contrast, if $\vec{k}_{pp}$ is used, the energy scale is much too low, resulting in unrealistically low cross sections and wrong analyzing powers. A consequence of the above procedure is that the energy at which the $pp \to d\pi^+$ reaction amplitudes are evaluated is constant for the $A(\vec{p},\pi^+)B$ reaction at a given bombarding energy, independent of $\vec{k}_0$ and of angle. An appreciation of the nature of this assumption can be obtained by noting that in the $A(\vec{p},\pi^+)B$ reaction the pion momentum with respect to the c.m. of the pn pair will be low for forward pion angles and high for backward pion angles, since the pn pair has a momentum strongly peaked in the forward direction. Hence, if the pion momentum with respect to the c.m. of the pn pair is used to define the energy scale, a strong angle dependence is introduced that raises the back-angle cross sections by an unphysical amount. The earlier assumption of a constant energy thus represents some averaging of these effects, a process that, in the real case, will be mediated by multiple scattering and distortions.

TABLE II. One- and two-nucleon nuclear structure expansion coefficients. The amplitudes ζ_{BC} for ^{13}C must be multiplied by the additional factor $1/\sqrt{78}$.

	Target nucleus			Residual nucleus			
Reaction	j_p	J_C	ζ_{AC}	$(j_p j_n)$	J	L	ζ_{BC}
^{2}H$(p,\pi^+)^3$H	$1s_{1/2}$	$\frac{1}{2}^+$	0.969		1	0	0.684
$\frac{1}{2}^+$	$1s_{1/2}$	$\frac{1}{2}^+$	0.969		1	2	0.141
	$1d_{3/2}$	$\frac{1}{2}^+$	−0.173		1	0	0.684
	$1d_{3/2}$	$\frac{1}{2}^+$	−0.173		1	2	0.141
^{3}He$(p,\pi^+)^4$He	$1s_{1/2}$	1^+	−0.682		1	0	−0.707
0^+	$1d_{3/2}$	1^+	0.153		1	0	−0.707
^{4}He$(p,\pi^+)^5$He	$1s_{1/2}$	$\frac{1}{2}^+$	1.000		1	1	0.193
$\frac{3}{2}^-$	$1s_{1/2}$	$\frac{1}{2}^+$	1.000		2	1	0.250
^{12}C$(p,\pi^+)^{13}$C							
0.00 MeV, $\frac{1}{2}^-$	$1s_{1/2}$	$\frac{1}{2}^+$	0.577	$1s_{1/2}1p_{1/2}$	0	1	0.500
sp	$1s_{1/2}$	$\frac{1}{2}^+$	0.577	$1s_{1/2}1p_{1/2}$	1	1	−0.866
	$1p_{3/2}$	$\frac{3}{2}^-$	0.816	$1p_{3/2}1p_{1/2}$	1	0	0.866
	$1p_{3/2}$	$\frac{3}{2}^-$	0.816	$1p_{3/2}1p_{1/2}$	1	2	0.866
	$1p_{3/2}$	$\frac{3}{2}^-$	0.816	$1p_{3/2}1p_{1/2}$	2	2	−1.118
3.09 MeV, $\frac{1}{2}^+$	$1s_{1/2}$	$\frac{1}{2}^+$	0.577	$1s_{1/2}2s_{1/2}$	1	0	−0.866
sp	$1p_{3/2}$	$\frac{3}{2}^-$	0.816	$1p_{3/2}2s_{1/2}$	1	1	0.866
	$1p_{3/2}$	$\frac{3}{2}^-$	0.816	$1p_{3/2}2s_{1/2}$	2	1	−1.118
3.85 MeV, $\frac{5}{2}^+$	$1s_{1/2}$	$\frac{1}{2}^+$	0.577	$1s_{1/2}1d_{5/2}$	2	2	0.646
sp	$1s_{1/2}$	$\frac{1}{2}^+$	0.577	$1s_{1/2}1d_{5/2}$	3	2	−0.764
	$1p_{3/2}$	$\frac{3}{2}^-$	0.816	$1p_{3/2}1d_{5/2}$	1	1	0.500
	$1p_{3/2}$	$\frac{3}{2}^-$	0.816	$1p_{3/2}1d_{5/2}$	2	1	−0.645
	$1p_{3/2}$	$\frac{3}{2}^-$	0.816	$1p_{3/2}1d_{5/2}$	2	3	−0.645
	$1p_{3/2}$	$\frac{3}{2}^-$	0.816	$1p_{3/2}1d_{5/2}$	3	3	0.764
	$1p_{3/2}$	$\frac{3}{2}^-$	0.816	$1p_{3/2}1d_{5/2}$	4	3	−0.866
3.68 MeV, $\frac{3}{2}^-$	$1p_{3/2}$	$\frac{3}{2}^-$	0.816	$1p_{1/2}1p_{1/2}$	1	0	1.000
2p-1h	$1p_{3/2}$	$\frac{3}{2}^-$	0.816	$1p_{1/2}1p_{1/2}$	1	2	1.000
6.86 MeV, $\frac{5}{2}^+$	$1p_{3/2}$	$\frac{3}{2}^-$	0.816	$1p_{1/2}1d_{5/2}$	2	1	0.088
2p-1h	$1p_{3/2}$	$\frac{3}{2}^-$	0.816	$1p_{1/2}1d_{5/2}$	2	3	0.088
	$1p_{3/2}$	$\frac{3}{2}^-$	0.816	$1p_{1/2}1d_{5/2}$	3	3	0.510
	$1p_{3/2}$	$\frac{3}{2}^-$	0.816	$1p_{1/2}2s_{1/2}$	1	1	−0.270
9.50 MeV, $\frac{9}{2}^+$	$1p_{3/2}$	$\frac{3}{2}^-$	0.816	$1p_{1/2}1d_{5/2}$	3	3	−0.500
2p-1h							
21.4 MeV, $\frac{13}{2}^-$	$1p_{3/2}$	$\frac{3}{2}^-$	0.816	$1d_{5/2}1d_{5/2}$	5	4	1.000
2p-1h							

B. Absorption effects

The optical potential appearing in the eikonal approximation for the scattering states is parametrized in the usual manner by a Woods-Saxon form factor with a diffuseness parameter a and real and imaginary depths V_0 and W_0. The imaginary part of this potential ($W_0 \leq 0$) results in absorption and the real part in a phase change, without altering the projectile momentum. When $V_0 = 0$ the mean free path of the projectile is simply related to W_0 by the expression $\lambda = \hbar v/2W_0$. More generally, combinations of V_0 and W_0 may be defined in terms of an approximately equivalent mean free path λ. Optical potential parameters appropriate for describing the propagation of protons and pions through a nuclear medium may be quite different from those that satisfy elastic scattering data. For this reason compatibility with absorption constraints was sought in the optical parameters that were used.

Recently, proton propagation in nuclei has been studied with the $(e,e'p)$ reaction [46]. Experimental transmissions for a nucleus like ^{181}Ta are greater by a factor of about 2 at 180 MeV than predictions of standard calculations. A new calculation of medium effects [47] that makes use of these new data shows that the mean free path of protons in symmetric nuclear matter at 200 MeV is about 4 fm. Figure 3 is a slightly modified and extended curve of the result presented in Ref. [47], which will be used in the present calculations. The horizontal scale will be interpreted as the total kinetic energy in the channel.

Extensive measurements of pion scattering and pion reactions have been made for the helium isotopes [48] and for heavier nuclei, including carbon [49]. From these data a universal curve was generated, as shown in Fig. 3, which gives the mean free path of pions in a nuclear medium as a function of the kinetic energy. This curve is consistent with, but not necessarily a unique representation of the scattering and reaction data. Nevertheless, it is adequate for present purposes in the calculations where absorption effects are studied.

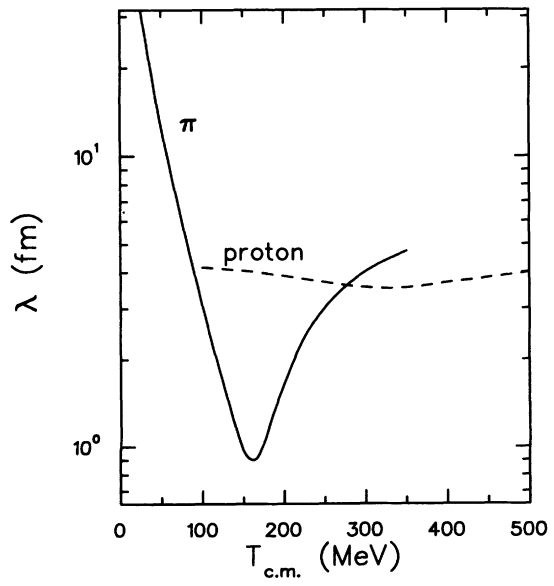

FIG. 3. Effective mean free path of protons and pions in nuclear matter as function of the total c.m. kinetic energy.

C. General features of predicted observables

A central feature of the predictions of this model is that the magnitudes of the analyzing powers for the $A(\vec{p},\pi^+)B$ reaction can be much greater than those for the $pp \rightarrow d\pi^+$ reaction. The restrictions imposed by angular momentum coupling dictate that the amplitudes for the $A(\vec{p},\pi^+)B$ reaction combine with different weightings than in the $pp \rightarrow d\pi^+$ reaction. Different final states would thus be expected to exhibit structure dependence of A_{N0}. Nevertheless, near threshold and up to about 200 MeV, the predictions are for a generally highly negative A_{N0} in the neighborhood of 60°–90° for most states. Overall, few of the other parameter choices have much influence on the analyzing powers, including absorption effects, although in the case of ^{2}H the D state is important.

The magnitudes of the predicted cross sections depend primarily on the energy scale defined for the calculation of the $pp \rightarrow d\pi^+$ reaction amplitudes, the degree to which momentum sharing can occur, and on absorption effects. The shapes of the angular distributions of the differential cross sections depend on several factors, among which the angular dependence of the momentum sharing is very important. Thus the details of the momentum distribution of the struck proton and the momentum states available to the recaptured pn pair play major roles. The significant momentum transfer variable is expressed through the quantity $\vec{q}$ defined by Eq. (9). A representation of the quantity $q' = |\vec{q} - \vec{k}_0|$ for several reactions is depicted in Fig. 4. Low values of q always favor antiparallel di-

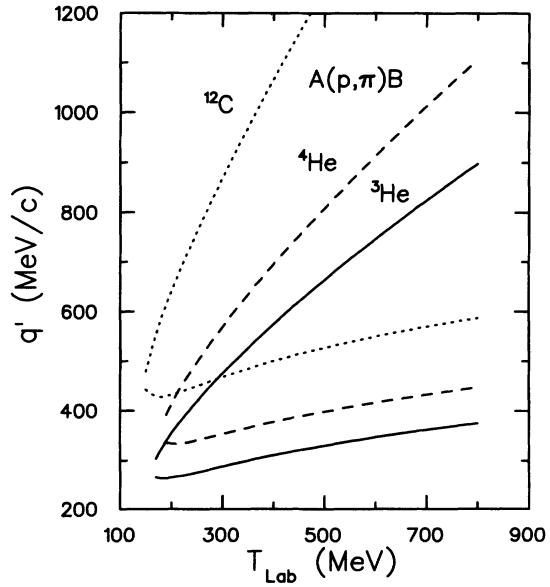

FIG. 4. Momentum transfer $q' = |\vec{q} - \vec{k}_0|$ as a function of proton bombarding energy. The lower (upper) branch for each curve corresponds to a pion scattering angle of 0° (180°).

rections for the incident and struck proton momenta. As well, near threshold where k_π is small, the angular dependence of q is modest, and its value small enough to yield a large value of the integral $I^R_{N'L\Lambda}(q)$ of Eq. (29). At higher energies the effect of $\vec{k}_\pi$ results in a greatly reduced integral at backward angles relative to forward angles and a correspondingly reduced differential cross section. Also important in the overall shape of the differential cross sections is the shape of the underlying $pp \to d\pi^+$ reaction cross section. This cross section, which is symmetrical about 90°, has a minimum at 90° which is about $\frac{1}{4}$ of the value at 0° for energies in the range of 400–500 MeV. The angular transformation that occurs in the calculation shifts this angle to about 60° in the $p + A$ frame.

The absolute magnitude of the differential cross section is generally not well defined in a plane wave model. Nevertheless, in the present case surprisingly consistent values of the normalization factor $N = \sigma_{\text{expt}}/\sigma_{\text{theory}}$, of the order of unity, were obtained over the whole range of nuclei and energies investigated. One notable exception to this case occurs for ^{12}C, as discussed in Sec. IV D. Normalization factors N applied to the calculated curves prior to plotting are given in each figure caption and are further discussed in Sec. V.

IV. RESULTS

A. ^{2}H($\vec{p}, \pi^+$)^{3}H

Results for a series of calculations for this reaction are shown in Fig. 5 for the angular distributions of the analyzing powers and in Fig. 6 for the differential cross sections. These calculations were performed with input conditions as previously discussed (standard input) with absorption effects in both the proton and pion channels set to zero. The initial and final state wave functions contained a D-state component of 6% and 7%, respectively. Because of the overall uncertainty in the theoretical energy scale, the calculations have been carried out at a number of energies in the vicinity of the experimental data. These data are from Ref. [50] at 277 MeV, from Ref. [51] at 330 MeV, and from Ref. [52] at

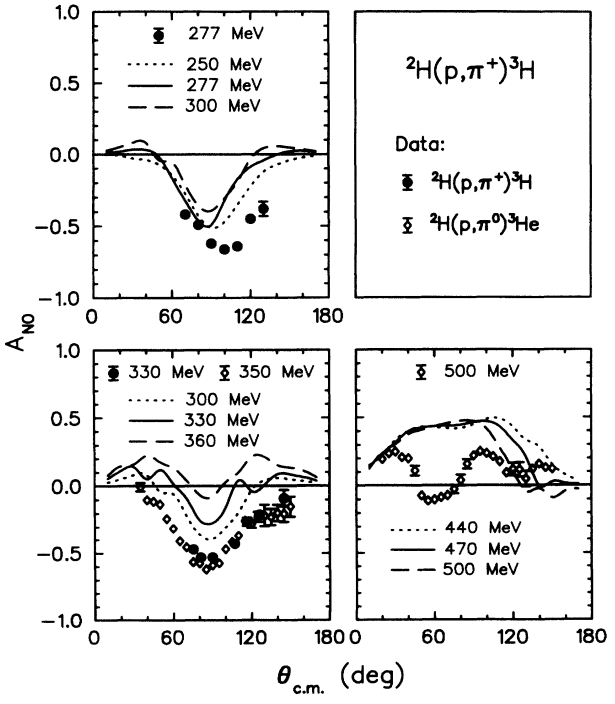

FIG. 5. Predictions of the model for the angular distributions of the analyzing powers for the ^{2}H(p, π^+)^{3}H reaction. The data at 277 MeV are from Ref. [50], at 330 MeV from Ref. [51], and at 350 and 500 MeV for the ^{2}H(p, π^0)^{3}He reaction from Ref. [52].

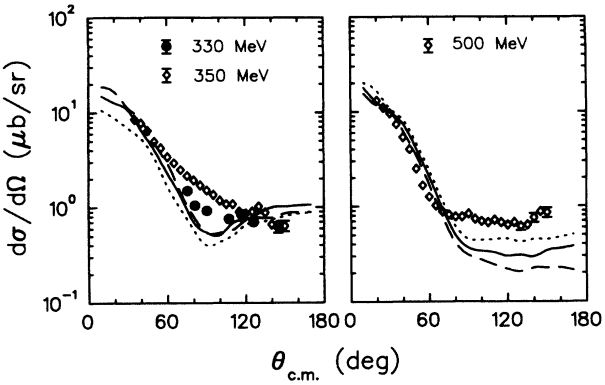

FIG. 6. Predictions of the model for the angular distributions of the differential cross sections for the ^{2}H(p, π^+)^{3}H reaction. The experimental data for the ^{2}H(p, π^0)^{3}He reaction have been multiplied by the isospin factor of 2. The calculated curves have been multiplied by the normalization factor $N = 0.38$. Other details are as given in Fig. 5.

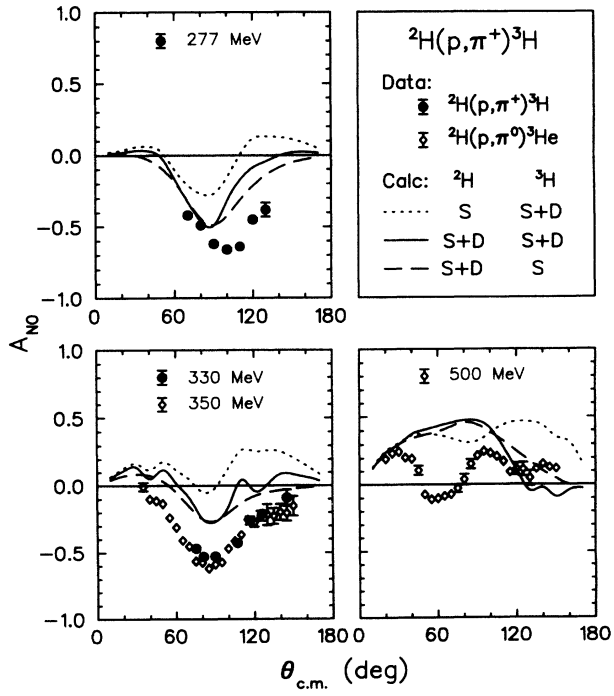

FIG. 7. Predictions of the model for the analyzing powers for the ^{2}H(p, π^+)^{3}H reaction as a function of D-state components in ^{2}H and ^{3}H. Other details are as given in Fig. 5.

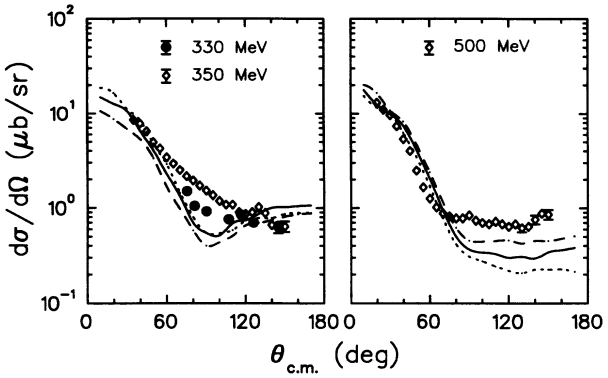

FIG. 8. Predictions of the model for the differential cross sections for the ^{2}H$(p,\pi^+)^3$H reaction as a function of D-state components in ^{2}H and ^{3}H. The calculated curves have been multiplied by the normalization factor $N = 0.38$. Other details are as given in Fig. 7.

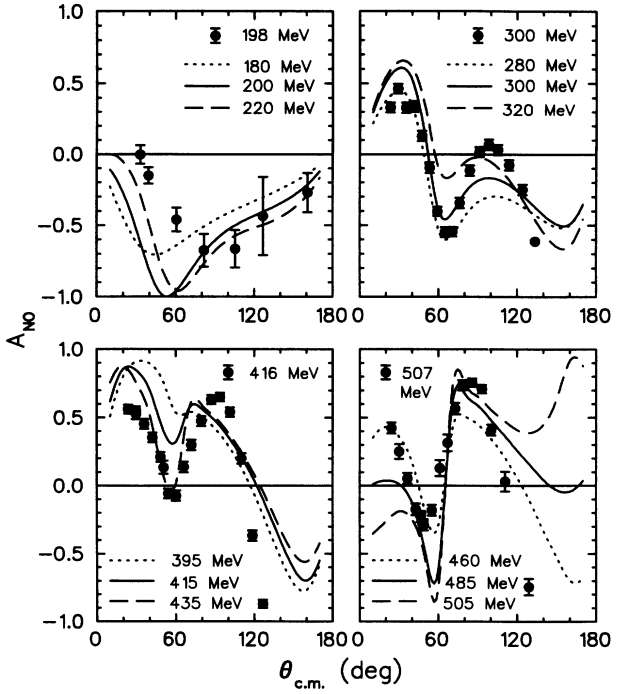

FIG. 9. Predictions of the model for the angular distributions of the analyzing powers for the ^{3}He$(p,\pi^+)^4$He reaction. The data at 198 MeV are from Ref. [53] and from Refs. [18,54] at the three other energies.

350 and 500 MeV for the ^{2}H$(\vec{p},\pi^0)^3$He reaction. Angular distributions for the (p,π^+) reaction below 500 MeV are fragmentary, and for this reason results for the (p,π^0) reaction have been used. For comparison of cross sections, the isospin factor of 2 was applied to the latter reaction.

The calculated analyzing powers in the neighborhood of 277 and 330 MeV are typically less negative than the experimental results, but possess the general character displayed by the data. A rapid energy dependence is noted in the predicted results in the range 300–360 MeV. At 500 MeV the calculated analyzing powers are very different from the ones observed experimentally. However, the 500 MeV differential cross sections shown in Fig. 6 are in reasonable agreement with experiment, although the plateau region beyond 70° is considerably below the data. Marked differences are evident between the (p,π^+) and (p,π^0) experimental cross sections at 330 and 350 MeV; the calculated results are thus broadly consistent with the data.

The calculations displayed in the two previous figures included a D-state component in both the ^{2}H target and the ^{3}H residual nucleus. If these components are not included in one or the other of these nuclei, the predictions, particularly for the analyzing powers, are considerably modified. This is shown in Fig. 7, where it is observed that omission of the D state in ^{2}H greatly increases the discrepancy between prediction and experiment. Omission of the D state in ^{3}H has a much smaller effect. On the other hand, effects on the cross sections are relatively small, as displayed in Fig. 8.

B. ^{3}He$(\vec{p},\pi^+)^4$He

Calculations for this reaction for a series of energies are shown in Fig. 9 for the angular distributions of the analyzing powers and in Fig. 10 for the differential cross sections. Absorption effects in both the proton and pion channels were set to zero. A D-state component of 7% was included in the target ^{3}He wave function. The data in these figures are from Ref. [53] at 198 MeV and from Refs. [18,54] at 300, 416, and 507 MeV. The experimental analyzing powers are observed to change very rapidly between 200 and 300 MeV and less rapidly thereafter. The model predictions tend to follow this pattern closely. At 200 MeV the predictions have a deeper minimum and are also shifted in angle from the minimum observed experimentally at 90°. For the higher energies, the positions of the maxima and minima in the analyzing powers are well reproduced, although their magnitudes show some discrepancies. The large negative values of A_{N0} at about 120° for 416 and 507 MeV are not reproduced, but here the momentum transfer is already quite large.

The calculated differential cross sections shown in Fig. 10 fit the shape of the experimental data quite well at 300 and 416 MeV, but are too flat at 200 MeV and too steep at 500 MeV. Relative magnitudes of the forward angle cross sections are well reproduced.

Sensitivity of these calculations to a number of assumptions made will now be considered. First, the effect of omitting the contribution from the pn unbound final state (through σ_{10}) has the effect of reducing the differential cross sections to values of 75%, 75%, 47%, and 29% of the magnitudes given in Fig. 10 for the energies of 200, 300, 415, and 505 MeV, respectively. The consequence is an increasing departure between the experimental data and calculated results as the energy is increased. Given the manner in which the contribution for the pn unbound final state is treated, no differences arise for the analyzing powers.

Second, the importance of the D-state component in

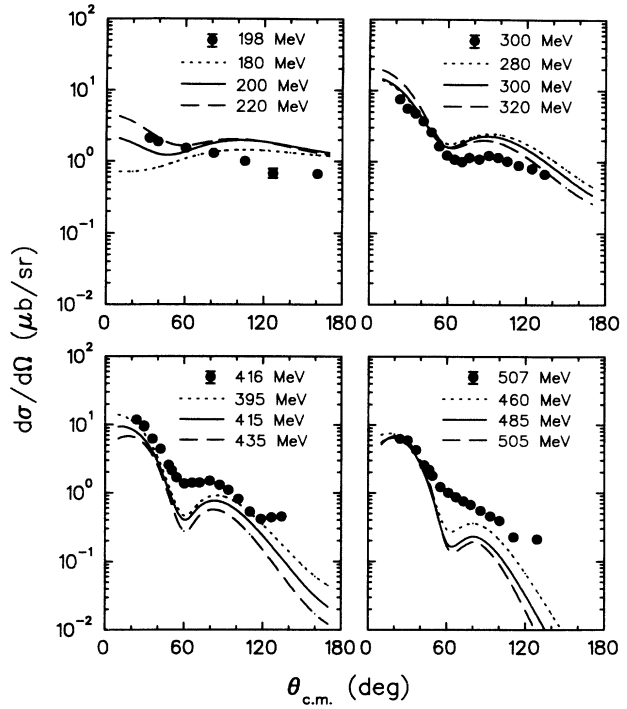

FIG. 10. Predictions of the model for the angular distributions of the differential cross sections for the ^{3}He$(p,\pi^+)^4$He reaction. The calculated curves have been multiplied by the normalization factor $N = 1.11$. Other details are as given in Fig. 9.

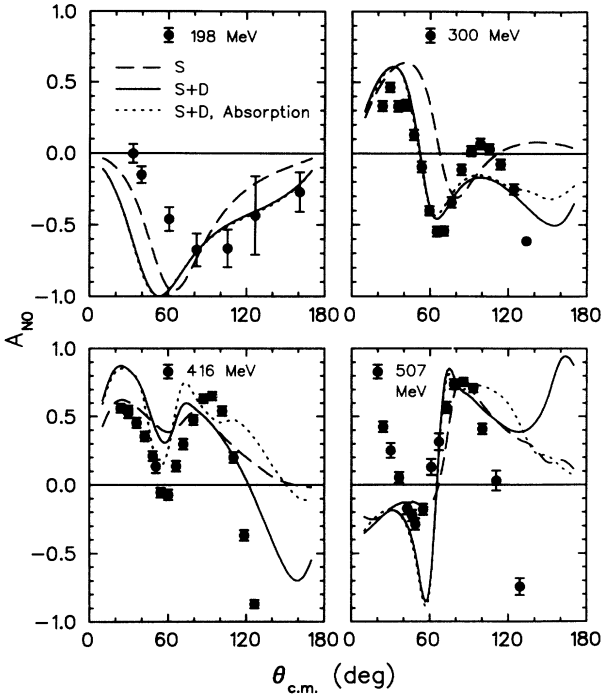

FIG. 11. Comparison of model predictions for the analyzing powers for the ^{3}He$(p,\pi^+)^4$He reaction as a function of D-state effects in ^{3}He and as a function of absorption in the incident and outgoing channels. Other details are as given in Fig. 9.

^{3}He is considered. Analyzing powers shown in Fig. 11, with and without this component included in the calculation, reveal that the positions of the maxima and minima are strongly affected. Without the D-state component, the disagreement between prediction and experiment grows markedly, especially for 300 and 416 MeV, where reasonable fits were otherwise obtained. Likewise, the predicted differential cross sections, shown in Fig. 12, fit the minima (or points of inflection) of the experimental data much better if the D state is included.

Finally, the effects of absorption are considered in calculations where the projectile mean free paths, as given by Fig. 3, are introduced. These mean free paths at bombarding energies of 200, 300, 415, and 505 MeV are, respectively, 4.0, 3.8, 3.6, and 3.9 fm for protons and 28, 3.1, 1.1, and 2.7 fm for pions. The very rapid change of the pion mean free path over this energy range can be expected to lead to pronounced effects, and this is indeed observed to be the case. However, except for the 415 MeV case, the effect is primarily in an overall reduction of the differential cross section, as shown in Fig. 12. At 200 MeV the differential cross section is reduced to 65% of its earlier value, at 300 MeV to about 42%, and at 505 MeV to about 40%. In addition, for the latter energy there is a noticeable enhancement at backward angles. For 415 MeV a large overall reduction at forward angles is observed, accompanied by a large enhancement at backward angles. Absorption effects lead to differences in the analyzing powers which are significant only at 415 MeV and to a lesser extent at 505 MeV, as shown

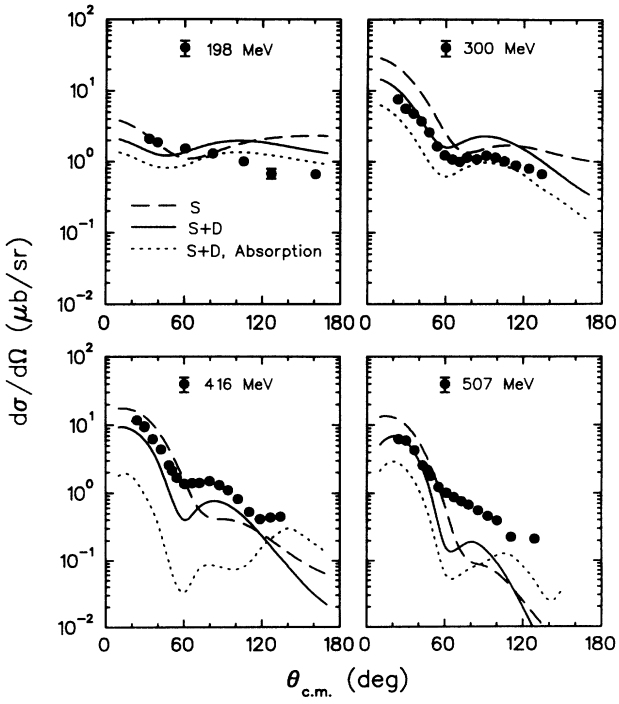

FIG. 12. Comparison of model predictions for the cross sections for the ^{3}He$(p,\pi^+)^4$He reaction as a function of D-state effects in ^{3}He and as a function of absorption in the incident and outgoing channels. The calculated curves have been multiplied by the normalization factor $N = 1.11$. Other details are as given in Fig. 10.

in Fig. 11.

The previous calculations investigating absorption effects are equivalent to using $V_0 = 0$ and $W_0 \neq 0$. Various combinations of potentials were explored which were equivalent in their attenuation factors. For example, the potential $V_{0p} = 20$ MeV, $W_{0p} = -14$ MeV, $V_{0\pi} = 0$ MeV, and $W_{0\pi} = -26$ MeV at 300 MeV produces a cross section about 30% greater than the above case. Other potentials could effect a 10%–20% reduction or a 10% forward-backward change in the shape of the differential cross section. In all cases these changes were not substantial, and all produced the same analyzing powers.

C. ^{4}He$(\vec{p},\pi^+)^5$He

Results for a series of calculations for this reaction are shown in Fig. 13 for the angular distributions of the analyzing powers and in Fig. 14 for the differential cross sections. The same conditions apply as for the calculations for ^{3}He, with absorption effects in both the proton and pion channels set to zero. In addition, the target ^{4}He nucleus was assumed to be pure $(1s_{1/2})^4$ and the final nucleus pure $(1s_{1/2})^4(1p_{3/2})^1$. Experimental results at the four energies of 240, 300, 400, and 500 MeV are from Furutani *et al.* [54]. What is striking in the experimental results is the general similarity in the shapes of the angular distributions for both A_{N0} and $d\sigma/d\Omega$ to those for ^{3}He. However, the cross sections for ^{4}He are typically larger by a factor of about 2. (Note that the cross sections for ^{4}He going to the unbound ^{5}He final state employed an integration cutoff at 4.44 MeV excitation of the $n + \alpha$ system, as discussed in Ref. [54].)

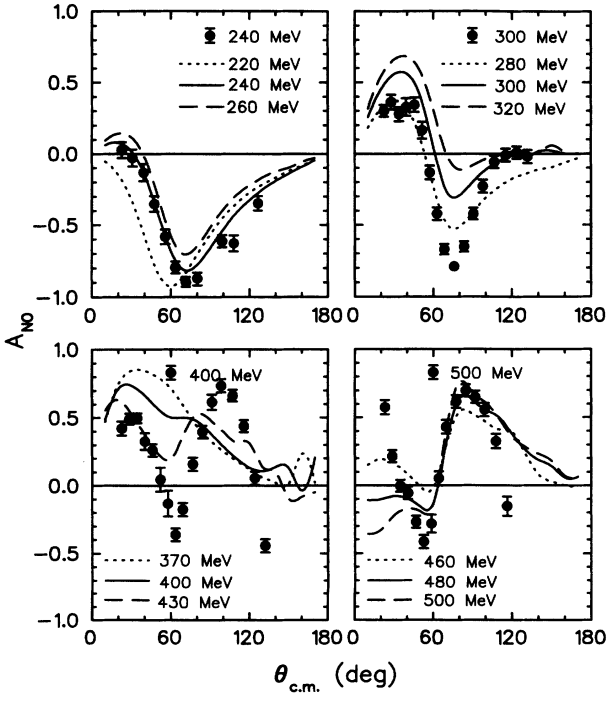

FIG. 13. Predictions of the model for the angular distributions of the analyzing powers for the ^{4}He$(p,\pi^+)^5$He reaction. The data are from Ref. [54].

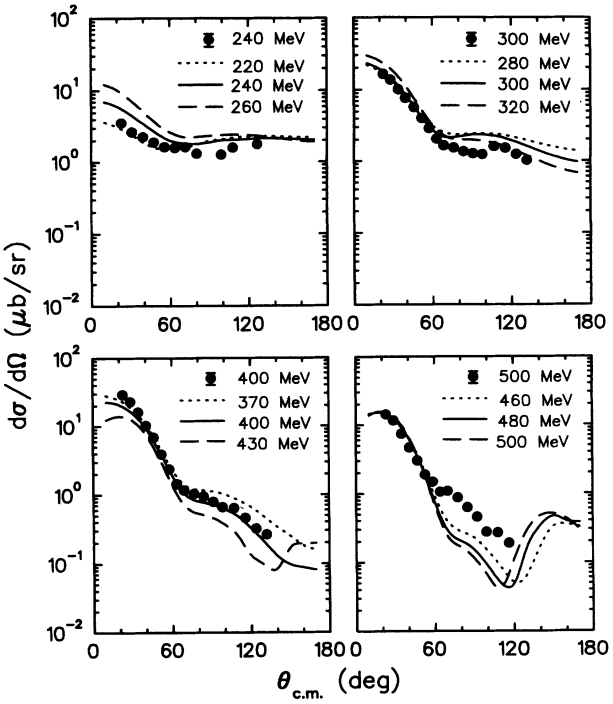

FIG. 14. Predictions of the model for the angular distributions of the differential cross sections for the ^{4}He$(p,\pi^+)^5$He reaction. The calculated curves have been multiplied by the normalization factor $N = 0.75$. Other details are as given in Fig. 13.

A good fit to the data for both A_{N0} and $d\sigma/d\Omega$ is observed at the lowest energy of 240 MeV, and fits at 300 MeV are comparable to those shown in Fig. 9 for ^{3}He. The calculated cross sections at 400 MeV still represents a good fit to the data, but the analyzing powers do not. Features of the latter A_{N0} are rather similar to those at 415 MeV in Fig. 11 when only the S state for ^{3}He is considered. Since the $(1s_{1/2})^4$ configuration in ^{4}He contains considerably higher momentum components than the $(1s_{1/2})^3$ configuration in ^{3}He, a plausible explanation is that the former nucleus is more adequately described as a $(1s)^n$ configuration for this reaction at low energy than is the ^{3}He nucleus.

The sensitivities of the calculated analyzing powers and cross sections to other assumptions made in the calculation (omission of pn unbound final state, absorption effects, etc.) were very similar to those discussed for ^{3}He, and little is added by providing these details. An aspect of the ^{4}He calculations, not present for ^{3}He, is the fact that the total angular momentum of the recaptured pn pair, $\vec{J} = \vec{L} + \vec{S}$, can have two values, namely, 1 and 2. Most of the strength comes from the $J = 2$ transition, but a change in the sign between the two corresponding amplitudes results in a large change in the analyzing powers, inconsistent with experiment.

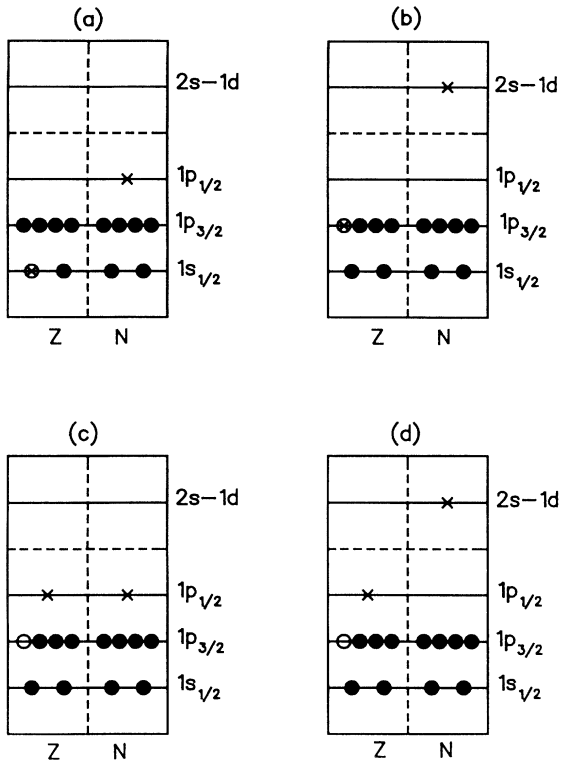

FIG. 15. Schematic of transition possibilities in the $pp \rightarrow d\pi^+$ model of the $A(\vec{p},\pi^+)B$ reaction (a),(b) for single-particle states and (c),(d) for two-particle–one-hole states. The symbol $\times$ indicates a proton or neutron transferred to previously unfilled levels and the symbol $\otimes$ the interaction with, and return of a proton to, its previously occupied level.

D. $^{12}C(\vec{p},\pi^+)^{13}C$

Nuclei with more than four or five nucleons present situations of increasing complexity. For example, for a nucleus like ^{12}C, interactions with protons from both the $1s$ and $1p$ shells contribute to the excitation of single-pariticle states like the $\frac{1}{2}^-$ g.s. On the other hand, excitation of two-particle–one-hole (2p-1h) states, like the $\frac{9}{2}^+$, 9.5 MeV state, involve only protons from the $1p$ shell. Figure 15 shows in schematic form the various transitions that may occur. Contributions from the $1s$ and $1p$ shells to a given final state are thus characterized by several L values (of different parties) and several values of J, the total angular momentum of the recaptured pn pair. Spectroscopic information for a number of states for this reaction is given in Table II. The simplest configurations only for these states were assumed in calculating the amplitudes, following the methods described in Refs. [32,33].

Contributions from the different (L,J) values give rise to complicated interference effects which are now examined for the transition to the g.s. of ^{13}C. Once more, standard input conditions were used in the calculations with absorption effects set to zero in both the proton and pion channels. The radial integral appearing in Eq. (29) then has the general form $q^L e^{-q^2/2\nu_B}$ for $N' = 0$ and $[1 - 2q^2/3\nu_B]e^{-q^2/2\nu_B}$ for $N' = 1$, $L = 0$. The q dependence of this integral results in a less rapid decrease as a function of angle of the differential cross section as L increases. In Fig. 16 results of calculations for the individual (L,J) transitions are shown, Fig. 16(a) when the target proton is from the $1s$ shell and Fig. 16(b) when the target proton is from the $1p$ shell. The angular distributions of the differential cross sections for the five separate transitions shown all exhibit different character. In particular, the two curves in Fig. 16(a), where identical dynamical factors apply, differ only because of angular momentum coupling ($J = 0, 1$). A similar statement applies to the two curves of Fig. 16(b) with $L = 2$ (and $J = 1, 2$). Indeed, the corresponding analyzing powers fall into three distinguishable patterns governed by $J = L - 1$, $J = L$, and $J = L + 1$. Finally, in Fig. 16(c)

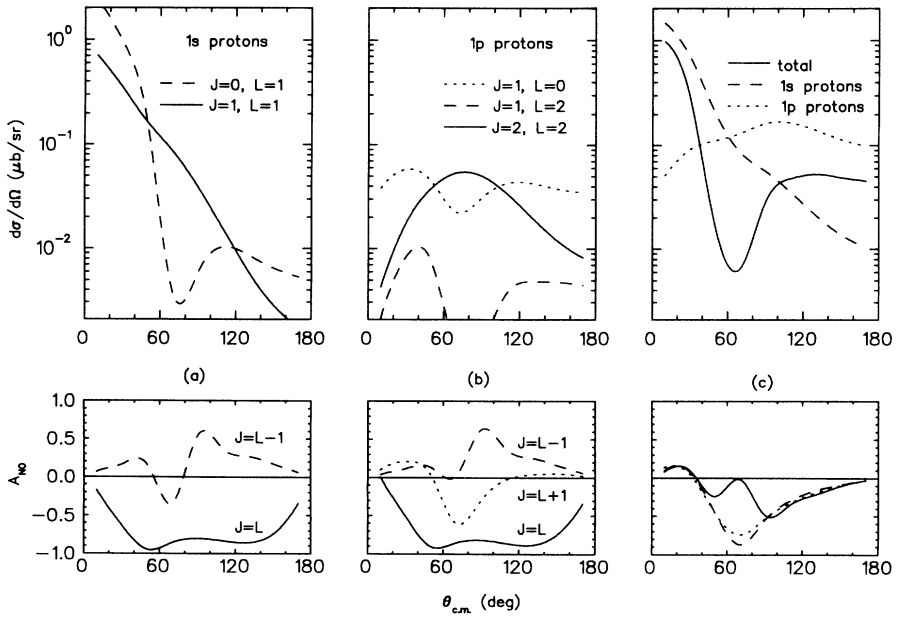

FIG. 16. Predictions of the model for the reaction $^{12}C(\vec{p},\pi^+)^{13}C$ g.s., $\frac{1}{2}^-$ at 200 MeV for individual (L,J) transitions (a) for interactions with $1s$-shell protons only and (b) for interactions with $1p$-shell protons only. The sum of contributions is shown in (c) separately for $1s$- and $1p$-shell protons, as well as their total. The calculated curves have been multiplied by the normalization factor $N = 1.35$.

the results are shown when the contributions from the $1s$ protons are added coherently and when the contributions from the $1p$ protons are added coherently. A final curve includes the coherent contributions from all five terms. The minimum in the differential cross section at $\approx 65°$ corresponds to destructive interference between contributions from the $1s$ and $1p$ protons. On the other hand, the angular distributions of the analyzing powers are almost identical for the $1s$ and $1p$ protons separately.

Unfortunately, unlike the results for ^{3,4}He, the results for ^{12}C are very sensitive to absorption effects. Comparisons are shown in Fig. 17 for three single-particle states. These single-particle states are all characterized by the presence of contributions from both $1s$ and $1p$ protons. The greater size of the ^{12}C nucleus compared with the ^{3,4}He nuclei, and the interference between the various contributions leads to a much greater sensitivity to details of the input parameters. Projectile mean free paths, as given by Fig. 3, of 3.9 fm for the proton and ≈ 15 fm for the pion were used in these comparisons. Dramatic enhancement of the back-angle differential cross sections is observed in all three cases when absorption is introduced. By comparison, the analyzing powers are much less strongly modified. Experimental data shown in this figure have been measured by Korkmaz *et al.* [17]. The unresolved 3.68 and 3.85 MeV doublet is estimated to comprise more than 80% the latter state. Calculations also confirmed a much smaller cross section for the 3.68 MeV state, but rather similar analyzing powers. In order to obtain the results in Fig. 17(a), the amplitudes for the contributions of the p-shell protons were reduced by a factor of 2, relative to those used in Fig. 16(c), as given in Table II. Differences between the relative s- and p-shell contributions is not unexpected when it is remembered that, in this case, harmonic oscillator functions are used to describe the momentum wave functions. Furthermore, the assumptions made regarding the structure of these states are oversimplified. Nevertheless, within the range of the two sets of calculations shown, a reasonable representation of the experimental data is obtained. It is interesting to observe that for the states referred to above the experimental data [17,55,56] from 190 to 250 MeV indicate a rapid rise followed by a rapid decrease in the analyzing powers in the angular range of about 80°–110°. This is clearly observed in the model calculations of Fig. 17, in the absence of absorption, and arises from interference between contributions from the $1s$- and $1p$-shell protons.

In contrast to the single-particle states just discussed, the two-particle–one-hole (2p-1h) states, where the contributions are from $1p$ protons only, display very different characteristics. The sensitivity of the calculated differential cross section angular distributions to absorption effects is much less than for the single-particle states, and the analyzing powers also are only weakly affected. Neither of the calculations for the 6.86 MeV, $\frac{5}{2}^+$ state shown in Fig. 18(a) is in good agreement with the experimental differential cross section, while for the 9.5 MeV, $\frac{9}{2}^+$ state, shown in Fig. 18(b), the cross section is fitted rather well, whereas the analyzing power is not. The observation of very strong states at high excitation in each of the ^{12}C$(p,\pi^+)^{13}$C and ^{13}C$(p,\pi^+)^{14}$C reactions is discussed in Ref. [17]. Because of the almost zero analyzing powers of these states, at 21.4 and 23.2 MeV excitation, respectively, they were judged to be anomalous when compared to all other transitions. For the present calculations, it has been assumed that the state in ^{13}C corresponds to the stretched configuration $(1d_{5/2})^2(1p_{3/2})^{-1}$ coupled to $\frac{13}{2}^-$. With these assumptions the results shown in Fig. 18(c) are obtained, which do indeed show small values of the analyzing powers and cross sections that resemble the experimental data. However, the predicted magnitude of the cross sections is relatively larger than

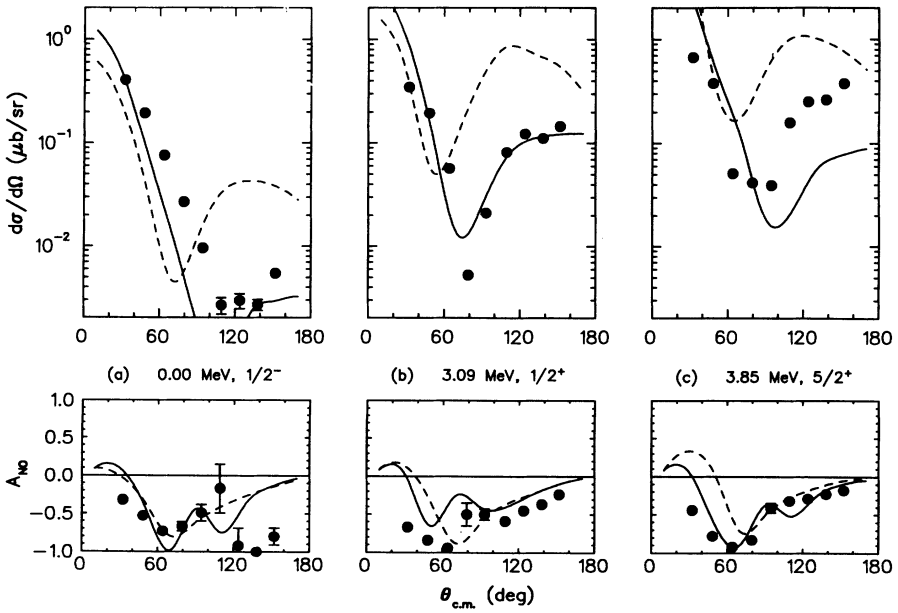

FIG. 17. Predictions of the model for the reaction ^{12}C$(\vec{p},\pi^+)^{13}$C at 200 MeV for several single-particle states, without absorption (solid line) and with absorption (dashed line) in the incident and outgoing channels. The data are from Ref. [17], where the 3.85 MeV state represents data from the unresolved 3.68 and 3.85 MeV doublet. The calculated curves have been multiplied by the normalization factor $N = 1.35$.

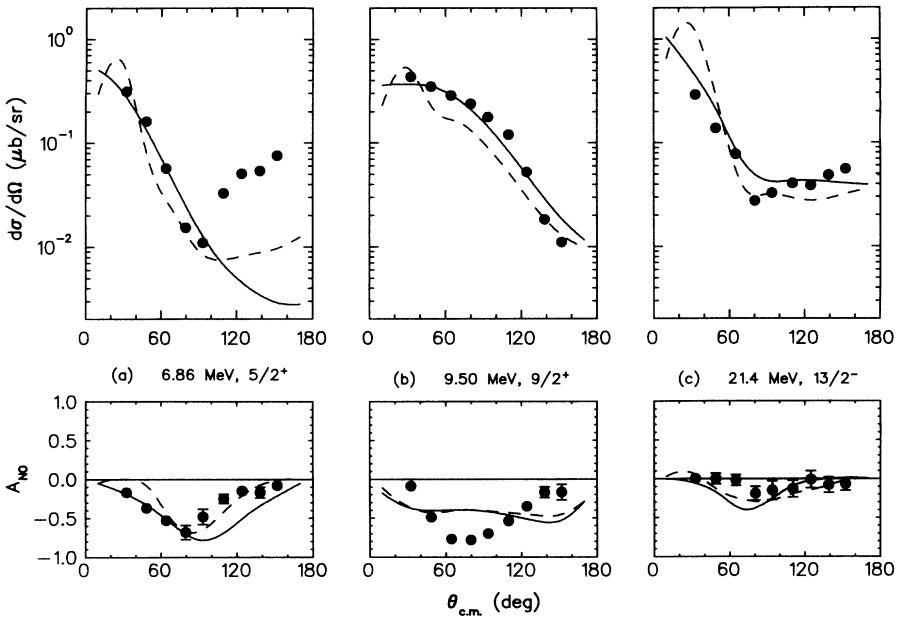

FIG. 18. Predictions of the model for the reaction $^{12}C(\vec{p},\pi^+)^{13}C$ at 200 MeV for several 2p-1h states, without absorption (solid line) and with absorption (dashed line) in the incident and outgoing channels. The data are from Ref. [17]. The calculated curves have been multiplied by the normalization factor $N = 1.35$ for (a) and (b) and by $N = 0.11$ for (c).

for the other states by an order of magnitude, requiring a normalization factor N of only 0.11.

Little success was obtained in studies of the energy dependence of the observables from 200 to 250 MeV for the g.s. The experimental cross section changes only slowly in this energy range, while the analyzing powers change dramatically [56]. Calculated results show rapid variations as a function of energy for both observables, but in a manner inconsistent with experiment. For the 9.5 MeV state, however, the energy dependence of the calculated observables is very gradual, which is consistent with the cross section data, but not with the analyzing power data [56].

Many of the qualitative observations with respect to the cross sections for the $^{12}C(p,\pi^+)^{13}C$ reaction are very similar in this model and the model of Kurath [31].

V. DISCUSSION AND CONCLUSIONS

In this paper an attempt has been made to put forward a simple phenomenological model of the $A(\vec{p},\pi^+)B$ reaction that incorporates our extensive knowledge of the $pp \to d\pi^+$ reaction. Most important in this model is the assumption that the $pp \to d\pi^+$ elementary process dominates over other $NN \to NN\pi^+$ processes in proton-induced nuclear pion production. Observables calculated in the model are the differential cross section and the analyzing power. Emphasis has been placed on correlating a wide body of experimental results through application of the model to (i) a broad range of target nuclei ^{2}H, ^{3,4}He, and ^{12}C, (ii) a wide range of proton bombarding energies, and (iii) cross section and analyzing power distributions covering a large angular range. The first point serves as a critical test of the model for diverse spin structures in the initial and final states, the second and third, as stringent dynamical tests as a function of energy and momentum transfer. No attempts have been made to obtain optimal fits to experimental data. In general, the model contains few adjustable parameters; indeed, with few exceptions as noted in the text, all the calculations were carried out under the same assumptions. This adds considerable weight to the conclusions. Many previous models have been applied in much more limited situations.

Overall, the calculations presented show that the model provides a rather good representation of the trends of the experimental data for the wide range of tests to which it has been subjected. In reference to the points made above, it is worth noting where limitations of the model may arise. First, as mentioned, only the NN isospin transition $1 \to 0$ has been included. However, the effective pp collision energies attain values where the NN isospin transition $1 \to 1$ may be far from negligible. Indeed, for proton bombarding energies of 200, 300, 410, and 500 MeV, the effective pp collision energies are often—depending on the struck proton momentum—in the range of 300, 450, 600, and 750 MeV, respectively. At these latter energies, the ratio $\sigma_{11}/\sigma_{10}^d$ is about 0.01, 0.15, 0.60, and 2.3, respectively. Interference of amplitudes from the $1 \to 1$ transition with those of the $1 \to 0$ transition will thus become of increasing importance as the energy is raised. Insufficient information presently exists on the details of the amplitudes of the former NN reaction for making quantitative estimates.

Second, one might well expect that the on-shell $pp \to d\pi^+$ reaction amplitudes involving pion-deuteron partial waves $l_\pi = 0, 1, 2$ will suffer modifications in the nuclear medium which increase rapidly with increasing value of l_π.

Third, the recaptured pn pair was restricted to internal orbital angular momentum $l' = 0$ [see Eq. (21)]. This was necessary in order to keep the calculation tractable. The neglect of the $l' = 2$ component may be important, particularly for a case like $^2H(p,\pi^+)^3H$, where the deep negative analyzing powers were not reproduced.

Fourth, the manner in which the energy scale is de-

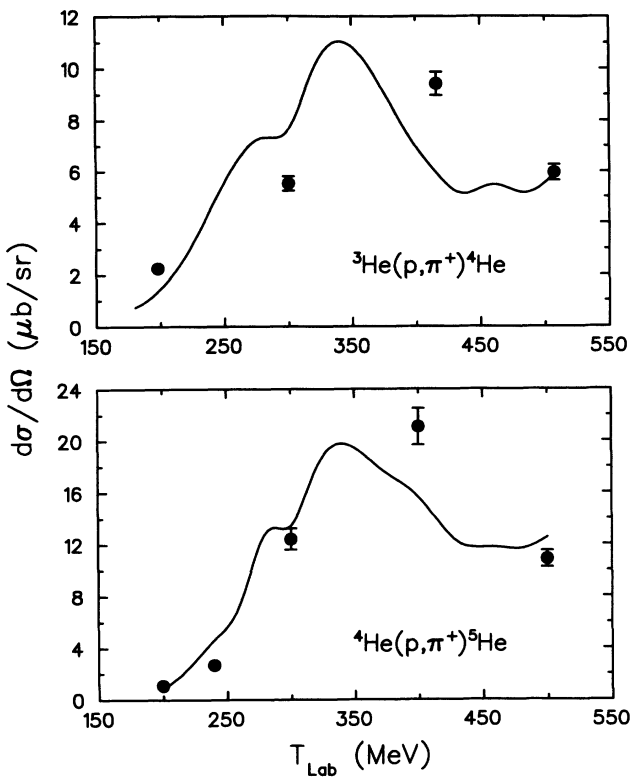

FIG. 19. Excitation functions at 30°. The 200 MeV points are from Refs. [53,57]. The calculated curves have been multiplied by the normalization factor $N = 1.11$ for ^{3}He and by $N = 0.75$ for ^{4}He.

fined in the model, in the calculation of the $pp \rightarrow d\pi^+$ reaction amplitudes, is rather arbitrary. The efficacy of this assumption is best judged in examining the excitation functions for the He(p,π)He reactions shown in Fig. 19. The model predicts that the peak in the excitation functions should occur at about 340 MeV, while the data suggest that it is closer to 400 MeV for both reactions. However, the range of the magnitudes of the 30° cross sections predicted is close to that actually observed. Two factors further complicate the interpretation of this figure; one is the neglect of absorption effects, which, if included, greatly increases the discrepancy because of its marked effect at 400 MeV (see Fig. 12). The other factor arises from the inclusion of the unbound pn σ_{10} contribution in the manner described. Omitting this contribution results in an increasing departure between experiment and prediction as the energy is raised. These observations suggest that the treatment of off-shell effects is inadequate—not a totally surprising conclusion.

Absorption effects were found to have a rather small influence on the calculated A_{N0} for the lighter target nuclei and only a moderate one for ^{12}C. Differential cross sections, on the other hand, were quite sensitive to these parameters, as expected, particularly in the neighborhood of 400 MeV on the He nuclei and at all energies for ^{12}C, because of its larger size. An exception to this latter case applies for the high spin states $\frac{9}{2}^+$ and $\frac{13}{2}^-$ where, presumably, the reaction is more strongly surface localized. Proper treatment of distortion effects is clearly important in many of these situations, but, unfortunately, difficult to incorporate into the present model.

Normalization factors $N = \sigma_{\text{expt}}/\sigma_{\text{theory}}$ were applied to all the calculated curves for $d\sigma/d\Omega$, as indicated in the various figures. In summary, these factors were 0.38, 1.11, 0.75, and 1.35 for the target nuclei ^{2}H, ^{3}He, ^{4}He, and ^{12}C, respectively. A single exception (to these values of order unity), for the putative $\frac{13}{2}^-$ state of ^{13}C, has been noted previously. For ^{2}H the value $N = 0.38$ provided good relative normalization at the two energies of 350 and 500 MeV, as shown in Fig. 6. For ^{3}He and ^{4}He, the above factors resulted in an energy dependence relative to the data, as previously discussed and shown in Fig. 19. The fact that these normalization factors are relatively constant and near unity is quite unexpected in a plane wave model. This must imply that much of the off-shell dependence of the reaction is rather well accounted for by use of the experimental $pp \rightarrow d\pi^+$ reaction amplitudes and the manner in which momentum sharing is built into the model. Moreover, several of the points discussed above—the definition of the energy scale, treatment of the unbound pn contribution, different ways of calculating the momentum wave functions, absorption effects, etc.—are likely to have a considerable influence on these normalization factors. In particular, it must be noted that these factors provide appropriate normalization of the model calculations to the data when absorption effects are set to zero. This is a somewhat puzzling result since the pion mean free path changes so dramatically over the range of energies investigated.

As a final comment on normalization, it is noted that the nuclear structure and other A-dependent factors of Eq. (24) lead to a cross section which, in the simplest case, is proportional to $|S^{1/2}_{AC}(1)S^{1/2}_{BC}(2)|^2$. In the general case, there is a coherent sum over all the initial and final state structure factors, with each term multiplied by appropriate dynamical and other factors.

New directions that can be explored to further test some of the assumptions in this model involve coincidence studies of the $(p,d\pi^+)$ reaction on nuclei. One such study has been reported [25], and other measurements are planned at higher energies at TRIUMF.

This work was supported in part by the Natural Sciences and Engineering Research Council of Canada.

[1] J. J. Domingo, B. W. Allardyce, C. H. Q. Ingram, S. Rohlin, N. W. Tanner, J. Rohlin, E. M. Rimmer, G. Jones, and J. P. Girardeau-Montaut, Phys. Lett. **32B**, 309 (1970).

[2] K. Gabathuler, J. Rohlin, J. J. Domingo, C. H. Q. Ingram, S. Rohlin, and N. W. Tanner, Nucl. Phys. **B40**, 32 (1972).

[3] S. Dahlgren, B. Höistad, and P. Grafström, Phys. Lett. **35B**, 219 (1971).

[4] B. Höistad, Adv. Nucl. Phys. **11**, 135 (1979).

[5] D. F. Measday and G. A. Miller, Annu. Rev. Nucl. Sci. **29**, 121 (1979).
[6] H. W. Fearing, Prog. Part. Nucl. Phys. **7**, 113 (1981).
[7] *Pion Production and Absorption in Nuclei—1981 (Indiana University Cyclotron Facility)*, Proceedings of the Conference on Pion Production and Absorption in Nuclei, edited by R. D. Bent, AIP Conf. Proc. No. 79 (AIP, New York, 1982).
[8] P. W. F. Alons, R. D. Bent, J. S. Conte, and M. Dillig, Nucl. Phys. **A480**, 413 (1988).
[9] M. J. Iqbal and G. E. Walker, Phys. Rev. C **32**, 557 (1985).
[10] E. D. Cooper and A. Matsuyama, Nucl. Phys. **A460**, 699 (1986).
[11] M. Dillig and M. G. Huber, Phys. Lett. **69B**, 429 (1977).
[12] H. J. Weber and J. M. Eisenberg, Nucl. Phys. **A312**, 201 (1978).
[13] P. W. F. Alons, R. D. Bent, and M. Dillig, Nucl. Phys. **A493**, 509 (1989).
[14] R. D. Bent, P. W. F. Alons, and M. Dillig, Nucl. Phys. **A511**, 541 (1990).
[15] G. M. Huber, G. J. Lolos, E. L. Mathie, Z. Papandreou, K. H. Hicks, P. L. Walden, S. Yen, X. Aslanoglou, E. G. Auld, and W. R. Falk, Phys. Rev. C **36**, 1058 (1987).
[16] G. M. Huber, G. J. Lolos, Z. Papandreou, K. H. Hicks, P. L. Walden, S. Yen, R. D. Bent, G. T. Emery, E. G. Auld, F. A. Duncan, and W. R. Falk, Phys. Rev. C **37**, 215 (1987).
[17] E. Korkmaz, S. E. Vigdor, W. W. Jacobs, T. G. Throwe, L. C. Bland, M. C. Green, P. L. Jolivette, and J. D. Brown, Phys. Rev. C **40**, 813 (1989); E. J. Korkmaz, Ph.D. thesis, Indiana University, 1987, and references therein.
[18] K. M. Furutani, W. R. Falk, F. A. Duncan, P. L. Walden, S. Yen, G. M. Huber, R. D. Bent, G. J. Lolos, and E. Korkmaz, Phys. Rev. C **44**, 1691 (1991).
[19] B. Höistad, M. Gazzaly, B. Aas, G. Igo, A. Rahbar, C. Whitten, G. S. Adams, and R. Whitney, Phys. Rev. C **29**, 553 (1984).
[20] B. Höistad, M. Bartlet, G. S. Adams, M. Gazzaly, B. Aas, G. Pauletta, F. Irom, K. Jones, and J. A. McGill, Phys. Lett. B **177**, 299 (1986).
[21] E. G. Auld, A. Haynes, R. R. Johnson, G. Jones, T. Masterson, E. L. Mathie, D. Ottewell, P. Walden, and B. Tatischeff, Phys. Rev. Lett. **41**, 462 (1978).
[22] E. Korkmaz, L. C. Bland, W. W. Jacobs, T. G. Throwe, S. E. Vigdor, M. C. Green, P. L. Jolivette, and J. D. Brown, Phys. Rev. Lett. **58**, 104 (1987).
[23] G. M. Huber, G. J. Lolos, R. D. Bent, K. H. Hicks, P. L. Walden, S. Yen, X. Aslanoglou, E. G. Auld, and W. R. Falk, Phys. Rev. C **37**, 1161 (1988).
[24] W. R. Falk, E. G. Auld, G. Giles, G. Jones, G. J. Lolos, W. Ziegler, and P. L. Walden, Phys. Rev. C **33**, 988 (1986).
[25] A. A. Cowley, P. G. Roos, J. J. Lawrie, F. D. Smit, J. V. Pilcher, S. V. Förtsch, G. F. Steyn, and G. C. Hillhouse, Phys. Rev. C **45**, 1745 (1992).
[26] D. J. Mack, P. G. Roos, H. Breuer, N. S. Chant, S. D. Hyman, F. Khazaie, B. G. Ritchie, J. D. Silk, G. S. Kyle, P. A. Amaudruz, Th. S. Bauer, C. H. Q. Ingram, D. Renker, R. A. Schumacher, U. Sennhauser, and W. J. Burger, Phys. Rev. C **45**, 1767 (1992).
[27] B. J. VerWest and R. A. Arndt, Phys. Rev. C **25**, 1979 (1982).
[28] M. Ruderman, Phys. Rev. **87**, 383 (1952).
[29] C. H. Q. Ingram, N. W. Tanner, J. J. Domingo, and J. Rohlin, Nucl. Phys. **B31**, 331 (1971).
[30] H. W. Fearing, Phys. Rev. C **16**, 313 (1977); **11**, 1210 (1975).
[31] D. Kurath, Phys. Rev. C **35**, 2247 (1987).
[32] N. K. Glendenning, *Direct Nuclear Reactions* (Academic, New York, 1983); Annu. Rev. Nucl. Sci. **13**, 191 (1963).
[33] I. S. Towner and J. C. Hardy, Adv. Phys. **18**, 401 (1969).
[34] J. R. Shepard and E. Rost, Phys. Rev. C **25**, 2660 (1982); D. F. Jackson, *Nuclear Reactions* (Chapman and Hall, London, 1970).
[35] D. V. Bugg, A. Hasan, and R. L. Shypit, Nucl. Phys. **A477**, 546 (1988); D. V. Bugg, *ibid.* **A437**, 534 (1985).
[36] B. Blankleider and I. R. Afnan, Phys. Rev. C **31**, 1380 (1985).
[37] W. R. Falk, E. G. Auld, G. Giles, G. Jones, G. J. Lolos, W. Ziegler, and P. L. Walden, Phys. Rev. C **32**, 1972 (1985).
[38] G. F. Wolters, in *Kinematics and Multiparticle Systems*, edited by M. Nikolić (Gordon and Breach, New York, 1968), p. 267; M. L. Goldberger and K. M. Watson, *Collision Theory* (Krieger, New York, 1975).
[39] R. Machleidt, K. Holinde, and Ch. Elster, Phys. Rep. **149**, 1 (1987).
[40] R. Schiavilla, V. R. Pandharipande, and R. B. Wiringa, Nucl. Phys. **A449**, 219 (1986).
[41] C. Marchand, M. Bernheim, P. C. Dunn, A. Gérard, J. M. Laget, A. Magnon, J. Morgenstern, J. Mougey, J. Picard, D. Reffay-Pikeroen, S. Turck-Chieze, P. Vernin, M. K. Brussel, G. P. Capitani, E. DeSanctis, S. Frullani, and F. Garibaldi, Phys. Rev Lett. **60**, 1703 (1988).
[42] M. B. Epstein, D. A. Krause, D. J. Margaziotis, A. Bracco, H. P. Gubler, D. K. Hasell, W. P. Lee, W. T. H. vanOers, R. Abegg, C. A. Miller, and A. W. Stetz, Phys. Rev. C **32**, 967 (1985).
[43] W. T. H. vanOers, B. T. Murdoch, B. K. S. Koene, D. K. Hasell, R. Abegg, D. J. Margaziotis, M. B. Epstein, G. A. Moss, L. G. Greeniaus, J. M. Greben, J. M. Cameron, J. G. Rogers, and A. W. Stetz, Phys. Rev. C **25**, 390 (1982).
[44] J. M. Negele, Phys. Rev. C **1**, 1260 (1970).
[45] P. Couvert, in *Proceedings of the Workshop on Studying Nuclei with Medium Energy Protons*, Edmonton, Alberta, Canada, 1983, edited by J. M. Greben, TRIUMF Proc. TRI-83-3, 287 (1983); in *Intersections Between Particles and Nuclear Physics (Steamboat Springs, Colorado)*, Proceedings of the Conference on the Intersections of Particle and Nuclear Physics, edited by Richard E. Mische, AIP Conf. Proc. No. 123 (AIP, New York, 1984), p. 689.
[46] G. Garino *et al.*, Phys. Rev. C **45**, 780 (1992).
[47] V. R. Pandharipande and S. C. Pieper, Phys. Rev. C **45**, 791 (1992).
[48] B. Brinkmöller *et al.*, Phys. Rev. C **44**, 2031 (1991); M. A. Khandaker *et al.*, *ibid.* **44**, 24 (1991); J. Binon *et al.*, Nucl. Phys. **A298**, 499 (1978).
[49] D. Ashery *et al.*, Phys. Rev. C **23**, 2173 (1981); K. A. Aniol *et al.*, *ibid.* **33**, 208 (1986).
[50] G. J. Lolos, E. G. Auld, G. L. Giles, G. Jones, B. J. McParland, W. Ziegler, D. Ottewell, and P. L. Walden, Nucl. Phys. **A422**, 582 (1984).
[51] G. J. Lolos, E. L. Mathie, G. Jones, E. G. Auld, G. L. Giles, B. J. McParland, P. L. Walden, W. Ziegler, and

W. R. Falk, Nucl. Phys. **A386**, 477 (1982).
[52] J. M. Cameron, P. Kitching, J. Pasos, J. Thekkumthala, R. Abegg, D. A. Hutcheon, C. A. Miller, S. A. Elbakr, and A. H. Hussein, Nucl. Phys. **A472**, 718 (1987).
[53] J. J. Kehayias, R. D. Bent, M. C. Green, M. A. Pickar, and R. E. Pollock, Phys. Rev. C **33**, 725 (1986).
[54] K. M. Furutani, W. R. Falk, H. Guan, J. R. Campbell, F. A. Duncan, P. L. Walden, S. Yen, G. M. Huber, R. D. Bent, G. J. Lolos, E. Korkmaz, A. Trudel, and A. Celler, Phys. Rev. C **50**, 1561 (1994), this issue.
[55] M. C. Green, Ph.D. thesis, Indiana University, 1983.
[56] G. J. Lolos, E. G. Auld, W. R. Falk, G. L. Giles, G. Jones, B. J. McParland, R. B. Taylor, W. Zeigler, and P. L. Walden, Phys. Rev. C **30**, 574 (1984).
[57] Y. LeBornec, L. Bimbot, M. P. Combes-Comets, J. C. Jourdain, F. Reide, A. Willis, and N. Willis, J. Phys. G **11**, 1125 (1985).